https://doi.org/10.5194/egusphere-2026-4899
Preprint. Discussion started: 11 September 2026

Response of vegetation hydroclimatic stress indicators to global warming and deforestation in the Amazon rainforest

Lucas Ferreira Correa[1], Sebastian Bathiany[2], Yiannis Moustakis[3], Julia Pongratz[1]

[1]Department of Geography, Ludwig-Maximilians-Universität München, Munich, 80333, Germany.

[2]Earth System Modelling Group, Department of Aerospace and Geodesy, TUM School of Engineering and Design, Technical University of Munich, Munich Climate Center, Ottobrunn, 85521, Germany.

[3]Department of Civil and Environmental Engineering, Imperial College London, London, SW7 2AZ, United Kingdom.

Correspondence to: Lucas Ferreira Correa (lucas.ferreira@lmu.de)

Abstract. The Amazon rainforest (ARF) plays a key role in regulating the global climate, sustaining exceptional biodiversity, and supporting the cultures of indigenous peoples and local communities. The ARF is also considered a tipping element, as deforestation and global warming may impose sufficient stress to trigger a transition to a tropical savanna state. However, the climate and vegetation responses to deforestation and global warming, as well as associated tipping thresholds, remain incompletely understood. Here, we examine the response of four hydroclimatic indicators to deforestation and warming and discuss their implications for forest stability. We performed four idealized ARF deforestation experiments with the Earth System Model MPI-ESM-HR at 2°C of global warming. These scenarios were compared against two intact-forest scenarios for pre-industrial climate and for 2°C warming. Our results show that deforestation of 25% of the forest area can lead to 70% being under significant hydroclimatic stress. The area under stress increases to 89% when combining 25% deforestation and 2ºC warming, exceeding the deforestation-only effects of 50% deforestation (82%). Mean Annual Precipitation (MAP) and Dry Season Length (DSL) show the strongest changes, but behave differently: MAP decreases strongly in and near newly deforested areas, while DSL increases across large forest regions downstream of the deforested areas. Although the rainforest remains stable in the model, the enhanced hydroclimatic stress would likely increase tree mortality in the real world if vegetation cannot adapt. Our results hence emphasize the risk of forest dieback at forcing levels that can be reached within the next few decades.

1 Introduction

The Amazon rainforest is an important element for Earth's climate and biodiversity and is also of major relevance culturally, being home for hundreds of indigenous groups. The rainforest efficiently recycles moisture (Eltahir and Bras, 1994), with around 20% of Amazon precipitation being transpired by trees in the region at least once (Staal et al., 2018), making land–

https://doi.org/10.5194/egusphere-2026-4899
Preprint. Discussion started: 11 September 2026

atmosphere interactions important for forest stability. When the total evapotranspiration flux is considered, different methodologies estimate that between 24% and 41% of the Amazonian precipitation originates in the basin (Staal et al., 2018). Previous studies have shown that annual rainfall could be used as an efficient control parameter for the stability of tree cover (Hirota et al., 2011; Flores et al., 2024). In this context, a reduction in annual precipitation could pressure a tropical forest system to transition to a savanna-like state.

This potential tipping point of the Amazon rainforest has become an important topic of discussion since studies have assessed the climate impacts of deforestation in the Amazon (Henderson-Sellers and Gornitz, 1984; Lean and Warrilow, 1989; Shukla et al., 1990; Nobre et al., 1991; Salati and Nobre, 1991; Lean and Rowntree, 1993). Cox et al. (2004) found a forest dieback in an early Earth system model with dynamic vegetation. More recent models show local nonlinear decline in carbon pools (Parry et al., 2022) and tree cover (Bultan et al., 2025) in CMIP6 projections, but no large-scale Amazon forest dieback. McDowell et al. (2018) have found that increasing temperature, vapor pressure deficit and forest fire occurrence are associated with tree mortality in tropical forests. Rising temperatures in the Amazon could also alter the energy balance and the circulation (Chagnon and Bras, 2005), which in some cases could increase precipitation locally (Negri et al., 2004; Changnon and Bras, 2005). On the other hand, climate change tends to decrease moisture availability at a larger scale, which can be amplified by land-atmosphere feedbacks. Due to the role of moisture transport from upwind to downwind regions, such feedbacks may expand regions of large forest mortality to downstream regions (Eltahir, 1996; Zemp et al., 2017).

The trees in the Amazon rainforest have, however, a significant adaptive potential. Nepstad et al. (1994) have shown that a large fraction of the trees in the Amazon depend on their deep root system to not be exposed to extreme hydrological stress, in an adaptive process that guarantees that the vegetation could still be productive during the extended dry periods. Esquivel-Muelbert et al. (2020) have found that in different parts of the Amazon, the trees developed different strategies to survive external forcings. Nevertheless, the results from Anderegg et al. (2019) indicate that in large areas of the Amazon, trees have already been experiencing climatic extreme conditions that go beyond their adaptive capacities. This is in line with results shown by Marengo et al. (2021) that indicate a dramatic increasing trend in dry season length and temperature in the Amazon region. This is particularly remarkable in the southern part and in the areas close to the so called “Arc of Deforestation”, a region that has been under strong pressure from deforestation in the last few decades, and that extends from the south/southwest part of the rainforest to the the northeastern part of the Amazon.

The most recent literature corroborates the narrative of a potentially approaching tipping point of the Amazon rainforest. The lowest estimates have hypothesized that an increase of 2°C in global mean temperature or the surpassing of 20-25% in deforested area could lead to irreversible changes in precipitation, dry season length or cumulative water deficit capable of leading the Amazon rainforest to surpass a tipping point (Jones et al., 2009; Nobre et al., 2016; Lovejoy and Nobre, 2019; Hirota et al., 2021). However, there are still large uncertainties about the existence of tipping points and thresholds, due to uncertainties in rainfall projections, the response of the rainforest to climate change, and the role of land-atmosphere feedbacks in response to forcing, as well as the lack of observational data (Hirota et al., 2021). As a result, the nonlinear and potentially cascading hydroclimatic responses of the Amazon rainforest to incremental deforestation, and their potential

https://doi.org/10.5194/egusphere-2026-4899
Preprint. Discussion started: 11 September 2026

effects on forest stability, remain poorly quantified. Our work aims to contribute to assessing rainfall projections in response to global warming and different levels of deforestation. For this purpose, we selected four vegetation hydroclimatic stress indicators (VHSI), and analysed their deviation from the stable scenarios under different levels of deforestation with stable global temperature and under a 2 degree global warming scenario. They were chosen so that they could indicate the hydroclimatic stress via water availability, land-atmosphere coupling, and how long and intense are the periods with limited water supply. The aim is to better understand the different hydroclimatic stress factors that the forest could be exposed to in the near future, identify the most severe changes and how they could lead to tree mortality and the consequent surpassing of a tipping point of the Amazon rainforest. More specifically, in this study we assess three features in different idealized deforestation scenarios: (1) the extent of the significantly hydroclimatically stressed forest, here defined by the amount of forest deforested, with forest probability (according to the method by Hirota et al., 2011) below 50% or with at least moderate standardized anomalies of Dry Season Length (DSL), Mean Climatological Water Deficit (MCWD) or Top 10 cm Soil Moisture (SM10); (2) the deviation of the VHSI from a reference climate in the Amazon region and the Cerrado; and (3) how the newly deforested areas compare with the untouched areas of the forest.

2 Methods and data

2.1 Vegetation hydroclimatic stress indicators

We select four hydroclimatic indicators to investigate the hydrological pressure exerted on the vegetation of the Amazon rainforest as a response to deforestation and warming: (1) Mean Annual Precipitation [MAP]; 2) Dry Season Length [DSL]; (3) Mean Climatological Water Deficit [MCWD]; and (4) Top 10 cm mean annual Soil Moisture [SM10]. They are relevant because they provide an overview on whether the trees are having access to enough water (MAP and SM10) and whether they have been exposed to long (DSL) and severe (MCWD) periods with limited water availability. We used MAP to assess the probability of the annual precipitation at eachgrid cellto sustain a stable tropical forest state. This was done using the empirical reconstruction approach by Hirota et al. (2011), where MAP is input in a logistic regression with regionalized coefficients (available in the referred paper) to calculate the probability of finding forest in a certain location. The result of this method (that is, an estimation of the likelihood of forest cover based on mean annual precipitation) is often used as a resilience indicator (e.g. Nian et al., 2024) and it is discussed throughout this manuscript as the forest cover probability - therefore, the later presented < 50% forest probability refers to the estimate using MAP, via this method.

DSL, defined here as the number of months with monthly precipitation below 100 mm, indicates the change in length of the dry season, whereas MCWD, defined as the most negative annual value of the cumulative monthly balance between precipitation and evapotranspiration, is used as a proxy for the intensity of the dry season. The increasing length and intensity of the dry season play an important role for tree mortality due to hydraulic failure (Aleixo et al., 2019; Mantova, 2022). Therefore, these indicators are fundamental to analyse the hydroclimatic stress the forest is exposed to under warming and deforestation. When the forest does not receive enough water via precipitation, it can still access water in the soil. The

https://doi.org/10.5194/egusphere-2026-4899
Preprint. Discussion started: 11 September 2026

top layers of the soil are also relevant for land-atmosphere coupling and precipitation recycling. For that reason, soil moisture is also relevant for the stability of the forest. Nepstad et al. (2007) performed an observational experiment in a small area in the eastern Amazon where they found a 3.4 times increase in tree mortality when plant available soil water decreased below specific thresholds. In this context, we use SM10 as an indicator of land responses to atmospheric changes because it responds more rapidly to hydroclimatic stress than deep soil layer moisture, while also serving as a proxy for soil water available to vegetation - especially relevant when precipitation is insufficient to meet moisture demand.

With these four indicators we intend to cover the most important hydroclimatic indicators that could lead to tree mortality, and potentially large-scale forest dieback. Their deviations from the control climate are analysed using standardized anomalies, following a similar methodology as used by Papastefanou et al. (2022). The standardized anomaly is the absolute anomaly normalized in units of standard deviation. This standard deviation is computed from the interannual variability of each indicator in the whole 60-year time period of the simulation. We also use the same thresholds for standardized anomalies as Papastefanou et al. (2022), classifying standardized anomalies from 0.5 to 2.0 (or -0.5 to -2.0) as moderate, anomalies from 2.0 to 2.5 (or -2.0 to -2.5) as severe, and anomalies beyond 2.5 (or -2.5) as extreme. These classifications are based on statistical indicators rather than direct vegetation metabolic responses. Nevertheless, several of the references suggest that stronger deviations from the average state are generally associated with stronger hydroclimatic impacts on vegetation (e.g. Allen et al., 2010; Grossiord et al., 2020).

For stress identification, we classify all forest areas as "significantly disturbed" where (a) forest has been completely removed as imposed by the scenario, (b) forest probability is below 50% using the MAP and the method by Hirota et a. (2011), or (c) at least moderate standardized anomalies of at least one of the other three (excluding MAP) VHSI. Note that the intensity classifications are non-exclusive - the fraction of the forest under extreme stress (standardized anomalies > |2.5|) is part of the fraction of the forest under at least moderate stress. Criterion (c) excludes areas already meeting one of the two previous criterions. Criterion (a) is simply referred to as forest removal, and criterions (b) and (c) as hydroclimatic stress. The remainder is classified as undisturbed forest.

2.2 Model and experimental setup

In this study, we apply the widely-used Earth System Model MPI-ESM-HR (Müller et al., 2018). The atmosphere component ECHAM6 and the land component JSBACH have a 0.9375 degree horizontal resolution, and the ocean component MPI-OM has a horizontal resolution of approximately 0.4 degrees. The atmosphere component has 95 vertical levels and convection is not explicitly resolved, but parameterized; details about the parameterization used can be found in the model documentation (Stevens et al., 2013). The land component has 11 plant functional types and 5 soil layers (Reick et al., 2021). We use the same version of MPI-ESM-HR used as part of CMIP6, which implies a wide range of evaluation studies and comparisons to other models exist (e.g. Müller et al., 2018; Gutjahr et al., 2019; Mauritsen et al., 2019; Hu et al., 2022). This model version, similarly to different models and previous versions of this model, has a well documented

https://doi.org/10.5194/egusphere-2026-4899
Preprint. Discussion started: 11 September 2026

negative bias in precipitation in the north or the Amazon (Müller et al., 2018). A more detailed discussion about the model performance in the Amazon region is presented in the following sections.

We performed six different experiments to investigate the response of the Amazonian climate to different scenarios. They combine different four deforestation levels and one warming scenario. We emphasize that the scenarios are not meant to represent any actual deforestation scenario, but rather aim to mimic the effect of tree mortality (due to human forcing of any kind), in order to study the effects on the remaining (in particular downstream) forest areas.

The experiments are:

- Pre-industrial control: A new realization of the CMIP6 piControl experiment, representing pre-industrial conditions with prescribed CO2 and land use representing the year 1850. From now on referred to as piControl.

- Stable 2 degrees warming: an experiment with stable global temperature 2 degrees warmer than piControl, and all other forcings being identical to piControl. From now on referred to as stableT_2K.

- Stable 2 degrees warming + 25% deforestation: Same as stableT_2K, but with the northeastern 25% of the tropical forest replaced with croplands. From now on referred to as stableT_2K_ARF25.

- Stable 2 degrees warming + 50% deforestation: Same as stableT_2K, but with the northeastern 50% of the tropical forest replaced with croplands. From now on referred to as stableT_2K_ARF50.

- Stable 2 degrees warming + 75% deforestation: Same as stableT_2K, but with the northeastern 75% of the tropical forest replaced with croplands. From now on referred to as stableT_2K_ARF75.

- Stable 2 degrees warming + 100% deforestation: Same as stableT_2K, but with 100% of the tropical forest replaced with grasslands*. From now on referred to as stableT_2K_ARF100. *The difference to the other experiments come from technical differences in the configurations and aim of the experiments, which are further discussed in this section. Implications are also further discussed.

When changing tree cover to grass or crops, we keep the relative area coverage ratio between C3 and C4 PFTs at each grid cell. The experiments with intact or fully removed forest (piControl, stableT_2K, and stableT_2K_ARF100) did not use dynamic vegetation (interactive changes in the area fractions of PFTs at any grid cell), as they were designed for a multi-model intercomparison requiring fixed vegetation conditions. The different model configurations are also the reason why complete deforestation (stableT_2K_ARF100) replaces tropical forest with grasslands, whereas the intermediate deforestation experiments replace forest with croplands. This approach is the only technical way to use the dynamic vegetation module for unchanged regions, while also ensuring that deforested areas remain deforested throughout the simulations (since prescribing natural grasses would make these gasses compete with forest and allow forest regrowth). In

https://doi.org/10.5194/egusphere-2026-4899
Preprint. Discussion started: 11 September 2026

MPI-ESM-HR, croplands and grasslands share identical albedo, vegetation height, and roughness parameters, but differ in productivity, with crops exhibiting stronger seasonality and more pronounced productivity extremes. Within the scope of this study, this difference may produce slightly higher evapotranspiration over croplands. However, long-term grid-cell mean evapotranspiration differs by at most 5% between croplands and grasslands, whereas replacing forest with either vegetation type consistently changes evapotranspiration by more than 20%. This fourfold (or greater) contrast demonstrates that the climatic impacts of forest removal exceed the differences associated with representing complete deforestation using grasslands rather than croplands. Because all deforestation scenarios were conducted under 2 °C global warming, the stableT_2K scenario was used as a reference to isolate the deforestation-only effect by comparison with deforested simulations. Additionally, the piControl scenario was employed as a second reference to assess the combined effects of deforestation and 2 °C warming on the four VHSI.

The experiments are concentration-driven, that is, CO_2 levels were prescribed to control the global mean temperatures. Therefore, the effects of the imposed forest cover changes only include biogeophysical effects. Biogeochemical effects from CO_2 forcing are included in the +2°C forcing between piControl and all other simulations. These stable temperature experiments were branched from the CMIP6 MPI-ESM-HR 1pctCO2 experiment, which imposes a 1% CO_2 increase per year. We identified the year where this CO_2 increase led to a 2 degree global warming (using 30 year moving means) and from that year we started the new experiments prescribing CO_2 concentrations to have stable global temperatures. To determine the CO_2 levels required to obtain stationary global mean surface air temperatures immediately at the transition from the 1pctCO2 simulation to the stableT_2K* simulations, we apply the protocol by Wood et al., (2026), which is an implementation of the TIPMIP protocol (Winkelmann et al., 2026; Jones et al., 2026) for concentration-driven models. The approach relies on a simplification of the ESM as a two-layed model (Geoffroy et al., 2013). As a result, temperature slightly overshoots the target warming level in the first decade of the stable temperature experiments (< 0.4 °C), but it stabilizes thereafter (see Wood et al. 2026 for details).

Figure 1 shows the forest cover for the experiments with any level of forest removal. For forest removal we selected a lat-lon box with boundaries 17°S to 13°N and 81°W to 43°W. This box was selected to cover all the Amazon rainforest in the model. For each deforestation level, we removed instantly the respective percentage of the total forest inside of this box. The forest removal in these experiments starts in the northeast of the Amazon, moving inland in the direction of the moisture transport from the Atlantic Ocean. Therefore, the patterns of deforestation are idealized and do not try to reproduce what has been observed in the real world. The choice of the progressive removal of entire regions of the forest is related to the fact that the more inland (i.e. downstream) the vegetation is, the more it relies on moisture that has been recycled by vegetation upwind (Zemp et al., 2017; Staal et al., 2018). Starting with this premise, Zemp et al. (2017) performed experiments to link vegetation patches by atmospheric water fluxes, and observed that via this link, the loss of part of the forest could be self-amplified, affecting regions downwind. Following the same idea, we remove the forest progressively from the beginning of the moisture inland transport aiming to verify whether we can identify a self-amplified effect of the deforestation downwind. The 2ºC global warming was chosen to represent a scenario of future warming, especially relevant considering that by 2025

https://doi.org/10.5194/egusphere-2026-4899
Preprint. Discussion started: 11 September 2026

parts of the Amazon have already been experiencing more than 1ºC of warming (Marengo et al., 2025). All the analysis presented in this study considers a box to represent the Amazon slightly different from the box considered for deforestation. This box had boundaries 13 ºS to 11 ºN and 80 ºW to 47 ºW. This was done to avoid transition areas between the Amazon and drier regions in the south and east when analysing hydroclimatic indicators. All results of Amazon averages or total Amazon area refer to these boundaries.

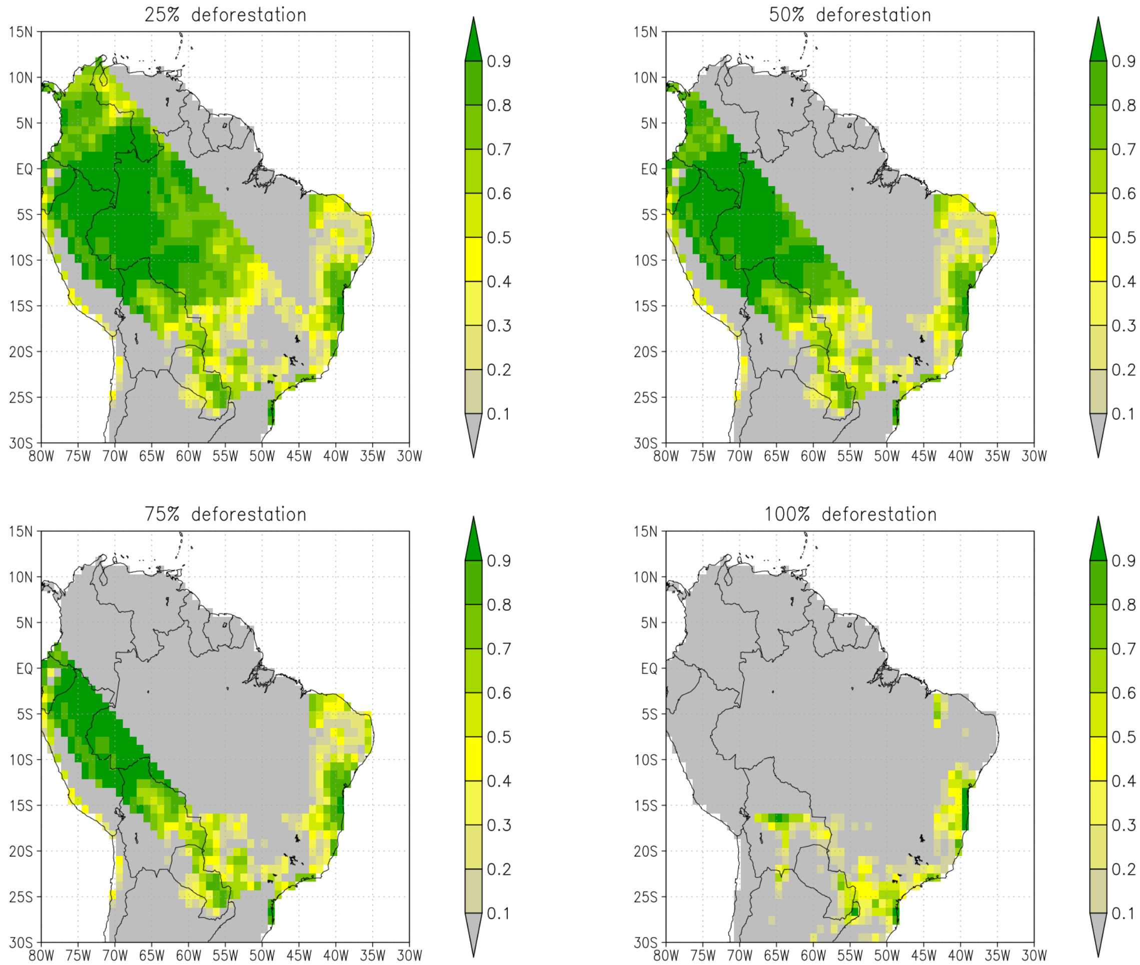

Figure 1 - Forest cover after imposing the deforestation scenarios used in this study. Colorbar indicates the cover fraction of the plant functional type "Evergreen Broadleaf Forest".

The intermediate deforestation experiments (stableT_2K_ARF25, stableT_2K_ARF50, and stableT_2K_ARF75) included dynamic vegetation, allowing vegetation cover to respond to environmental changes and enabling the assessment of potential vegetation shifts. Each experiment was run for 60 years, and the full simulation period was used to compute the averages presented in this study. Only minor changes in vegetation cover were detected, representing less than 2% of the total

https://doi.org/10.5194/egusphere-2026-4899
Preprint. Discussion started: 11 September 2026

vegetation cover. Several studies have discussed the stability of physical models and their tendency to overestimate vegetation stability and underrepresent abrupt transitions (e.g. Valdes, 2011; Liu et al., 2017). Consistent with this, a pre-industrial spin-up simulation with dynamic vegetation (not shown) revealed that grid cells with a strong negative precipitation bias (MAP < 500 mm year^{-1}) only stabilized after losing approximately half of their initial forest cover (~80–95%), leaving most grid cells with forest cover exceeding 40% after 60 years. However, Hirota et al. (2011) showed that such precipitation levels are associated with tree cover below 20% in more than 95% of real-world observations. This discrepancy indicates that the model exhibits an inherent tendency toward overly stable vegetation states under reduced precipitation. Therefore, we do not discuss simulated changes in forest cover, but instead focus on the hydroclimatic stress experienced by the vegetation and its implications for forest cover under real-world conditions. This approach is further supported by the extensive literature using one or more of the four indicators analysed here to investigate vegetation stress and hydroclimatic impacts (e.g. Aragão et al., 2007; Lewis et al., 2011; Good et al., 2015; Guan et al., 2015; Muller-Landau et al., 2021; Xu et al., 2022; Williams et al., 2025; Wunderling et al., 2026).

2.2 Comparison between model and observations

MPI-ESM has been evaluated in previous studies and model intercomparisons. Specifically, the model generates a physically meaningful response to idealized deforestation forcing, which is qualitatively comparable to results from other models (e.g. Boysen et al., 2020). To put the responses to CO_2 and deforestation forcing shown in later sections into historical context, we here qualitatively assess the performance of the model in representing the past changes in MAP and DSL, which are a combination of internal variability and forced response.

For this analysis, we used the gridded precipitation data from the Global Precipitation Climatology Center (GPCC; Schneider et al., 2022). This product integrates rain-gauge observations into gridded data, not including data from ships or buoys; therefore it is limited to continental areas. We used the monthly product at 0.5 degree spatial resolution. We compared this product (hereafter referred to as observations) with the historical MPI-ESM-HR simulation used in CMIP6 in terms of changes from an early period (1940-1969) to a late period (1985-2014). As the late period has larger influences from global warming and deforestation, our analysis aims to assess (i) whether the model exhibits unrealistic changes relative to observations and (ii) to how it reproduces the observed direction and magnitude of precipitation and dry-season-length changes between the periods, to the extent that these changes emerge from internal variability.

Figure 2 shows the differences in MAP and DSL between the late and early 30-year period for observations and simulations. We also highlight four subregions for visual guidance and for additional significance testing. The smaller boxes at the eastern (referred to as Eastern Arc) and southern (referred to as Southern Arc) transition areas of the Amazon cover parts of the Arc of Deforestation. The larger box south of 15ºS (from now on referred to as Downstream) covers a large area downstream of the Amazon moisture transport. Finally the large box in central Amazonia (referred to as Central region) covers a central area of the forest that has experienced lower deforestation rates compared to the Eastern and Southern Arc areas, and is not downstream of largely deforested areas.

https://doi.org/10.5194/egusphere-2026-4899
Preprint. Discussion started: 11 September 2026

Overall, in tropical South America in general, we find that the typical magnitude of changes is smaller in the model compared to observations, especially for MAP. This is likely due to the fact that the model underestimates the magnitude of internal climate variability. The ratio between median simulated-to-observed early-late period change for MAP was 0.34, 0.37 and 0.55 for the Eastern Arc, Southern Arc and Downstream region, respectively. For DSL these values were 0.50, 0.44 and 0.53, respectively. The observed pattern of MAP changes shows at least some similarity to trend assessments in previous studies (e.g. Cattelan et al., 2025; Cui et al., 2026), with increased precipitation in the central to eastern Amazon, and decreases in the south-eastern part of the arc of deforestation. Also, the historical simulation with MPI-ESM-HR shows some qualitative similarity to the observed changes, within the four selected regions, but also on the continent overall. Consequently, the sign of the changes in model and observations agrees at many grid cells, and also in all regional averages and for both indicators (MAP and DSL), except in the central region which is neither affected by substantial deforestation forcing nor located downstream of deforested areas (see Table 1). It also has to be kept in mind that observational datasets differ in the sign of precipitation trends in large parts of the central Amazon (Cattelan et al., 2025).

To assess changes between the two time periods, we applied Welch's two-sample t-test to the annual regional means, testing whether the mean values differed significantly between the early and late periods while allowing for unequal variances. We here did not take into account that spatial correlations between grid cells and temporal autocorrelation to some extent violate the test assumptions; however, previous studies do show that at least the decreased MAP in the southern Amazon region is significant (Cui et al., 2026).

The only region where we find statistically significant differences in both MAP and DSL observations between early and late periods is the downstream region (Table 1). We interpret that there is a distinguishable forced signal that the historical simulation could potentially reproduce. Therefore, we evaluate whether the historical simulation reproduces this signal in this region using three complementary spatial metrics: the spatial correlation between simulated and observed changes, the fraction of grid boxes with matching change signs, and the normalized centered root mean squared error (NCRMSE).

To assess whether the simulated changes exceeded those expected from internal climate variability, we used the pre-industrial control simulation to generate empirical distributions of the evaluation metrics under unforced conditions. Specifically, hundreds of independent 30-year change fields were randomly sampled from the pre-industrial control simulation and, one at a time, compared with the fixed historical simulation. For each comparison, the spatial correlation, normalized centered root mean squared error (NCRMSE), and proportion of grid cells with agreement in the sign of change were recalculated, thereby generating null distributions representing the level of agreement expected if the comparison were driven solely by internal variability. The values obtained from the comparison between the historical simulation and the observed change field were then compared with these null distributions, and p-values were calculated as the proportion of pre-industrial realizations exhibiting equal or stronger agreement (higher spatial correlation and sign agreement, or lower NCRMSE) than the historical simulation–observation comparison. This procedure assesses whether the agreement between the historical simulation and the observations is greater than would be expected from internal climate variability alone.

https://doi.org/10.5194/egusphere-2026-4899
Preprint. Discussion started: 11 September 2026

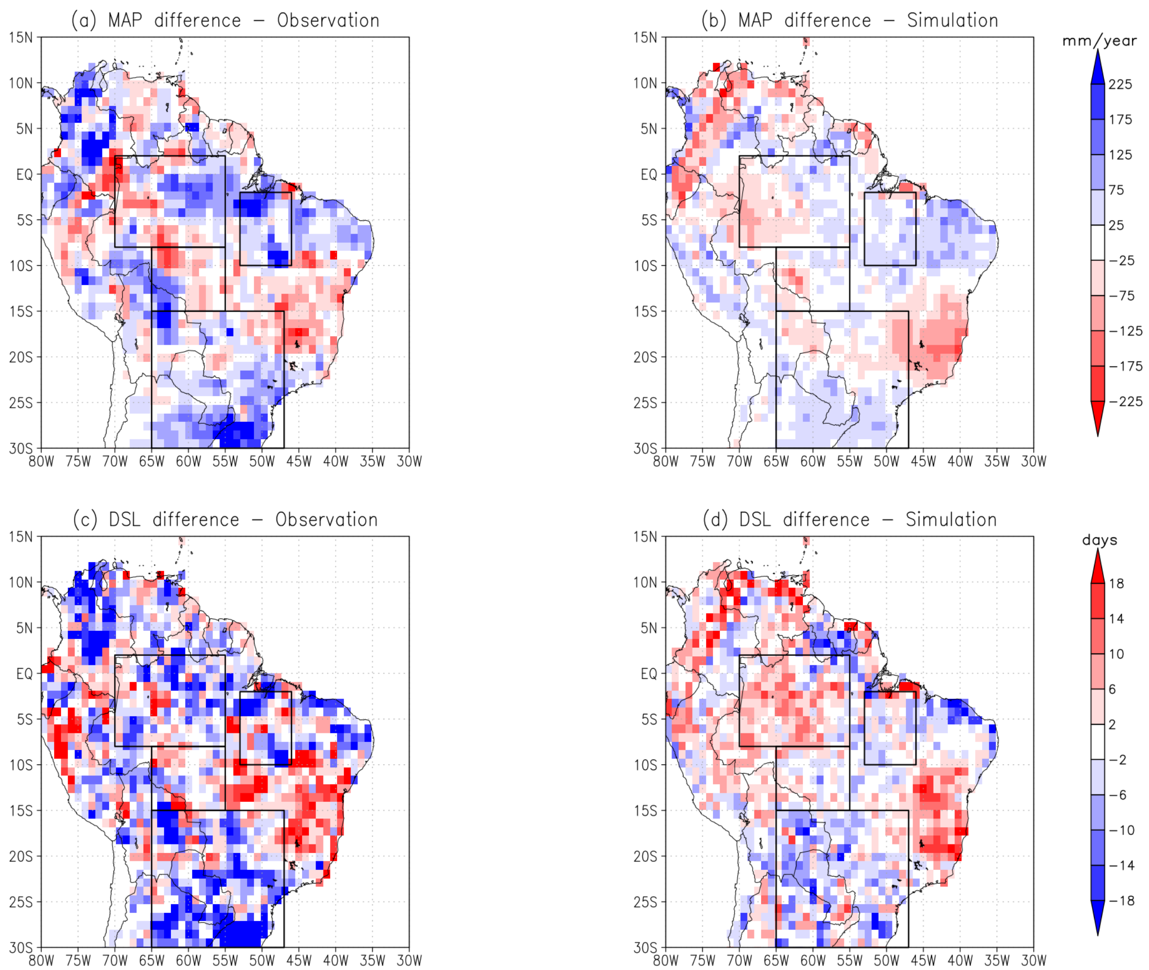

Figure 2 - MAP differences (in mm/year) between early (1940-1969) and late (1985-2014) periods from (a) observational (GPCC reanalysis), and (b) model (MPI-ESM-HR historical CMIP6 simulation) data; (c) and (d) show the same but for DSL differences (in days) respectively. Boxes indicate the Central, Eastern Arc, Southern Arc and Downstream regions.

		Eastern Arc	Southern Arc	Downstream	Central
Early-late difference (p)	MAP observation	**96.9 (0.0453)**	-4.1 (0.9067)	**59.9 (0.0295)**	12.0 (0.7512)
	MAP simulation	25.5 (0.6069)	-10.2 (0.7902)	12.1 (0.6948)	-7.4 (0.8805)

https://doi.org/10.5194/egusphere-2026-4899
Preprint. Discussion started: 11 September 2026

	DSL observation	-4.7 (0.1987)	0.4 (0.8907)	**-9.0 (0.0405)**	-3.3 (0.3437)
	DSL simulation	-0.8 (0.8531)	0.1 (0.9901)	-2.6 (0.5096)	3.9 (0.4155)

Table 1 - Spatial average MAP (in mm/year) and DSL (in days) changes from the mid-20th century (1940-1969) to the turn of century (1985-2014) for four regions (Eastern Arc, Southern Arc, Downstream and Central). The p-value of each difference is shown in parentheses. Statistically significant differences at the 5% level are highlighted in bold.

As mentioned above, the comparison shows that only the Downstream region exhibits statistically significant differences between the early and late periods in both MAP and DSL observations. This is therefore the only region where a robust forced signal can be identified, allowing an assessment of whether the historical simulation reproduces the observed response. For all other combinations of region and index where a significant deforestation forcing is expected (Eastern and Southern Arc), the simulated and observed changes have the same sign, although the simulated changes are consistently smaller in magnitude. However, because the observed changes are not statistically significant, it is not possible to determine whether this apparent agreement reflects a correct reproduction of a forced signal or is indistinguishable from internal variability. In the Central region, where no deforestation-induced signal is expected, the simulated and observed changes have opposite signs for both MAP and DSL.

We therefore further assessed the model performance in the Downstream region. For MAP, the spatial correlation (r) between historical simulation and observations equals 0.3348 ($p = 0.1131$). 70.19% of the gridboxes agree in sign ($p = 0.0611$) and the NCRMSE equals 0.9482 ($p = 0.0385$). For DSL, $r = 0.0741$ ($p = 0.1923$), 62.4% of the gridboxes agree in sign ($p = 0.0747$) and NCRMSE = 1.0716 ($p = 0.0023$). The results of the sign agreement and NCRSME indicate with higher than 90% confidence that for both MAP and DSL, the model is capable of correctly reproducing a forced signal. However, the low spatial correlation (even though also higher than most pre-industrial realizations) indicates that this agreement is stronger at the regional than at the grid level.

Overall, the results indicate that 1. the model is not significantly in conflict with observed changes over time, 2. the model likely underestimates internal variability (and potentially even the forced response). At the same time, our idealized experiments magnify the effects of deforestation in comparison to the real world, given that we completely remove large areas of the forest at the beginning of the inland moisture transport, largely affecting also downstream areas. We will see in the results below, that such forced changes are substantially larger compared to historical changes which already featured substantial droughts and tree mortality (Chambers et al., 2025).

https://doi.org/10.5194/egusphere-2026-4899
Preprint. Discussion started: 11 September 2026

3 Results

3.1 Hydroclimatic stress from deforestation

Figure 3 presents the Amazon-wide averages of the four VHSI across all deforestation scenarios. A primary feature is the nonlinearity of the response to increasing forest loss at least in some deforestation increments and indicators. This behavior is somewhat evident in the intermediate experiments, where forest is consistently replaced by croplands (therefore the incremental responses are not an artifact of the type of replacement vegetation). In general, a common pattern can be observed in MAP, SM10 and DSL: all show strong changes at 25% and 50% deforestation, followed by stabilization after 50% and large changes in the final 25% increment towards complete deforestation. MCWD exhibits the largest response in the first 0–25% deforestation increment, with an 5.6% reduction (more negative values indicating stronger deficit), whereas SM10 shows the smallest change (−1.3%). Following an additional 25% forest removal (totaling 50%), changes in SM10 and DSL slow (−1.2% and +2.2%, respectively), and MCWD remains approximately stable. Precipitation is the only variable showing an accelerated response between 25–50% deforestation (−4.2%) compared to 0–25% (−2.3%). The 50-75% deforestation interval shows stable conditions for DSL, SM10 and precipitation. MCWD, on the other hand, shows the largest change in this deforestation interval (~6% deficit increase in absolute values). In the final deforestation increment, from 75% to 100%, DSL, SM10 and precipitation show the largest changes, with 8.3% increase in DSL, a 10.6% decrease in MAP and 3.0% decrease in SM10. The differences in the land surface parameters (such as albedo, roughness length and productivity) between crops and grasslands are small compared to grass/crop versus forest, therefore they contribute only marginally to these effects, making it unlikely that this is the cause for the largest changes observed. Nevertheless, the possibility that regional characteristics influenced the response cannot be excluded. Unlike the other indicators, MCWD became less negative in the final deforestation increment, indicating a weaker intensification of dry-season conditions. Because MCWD reflects the combined effects of precipitation and evapotranspiration, this behavior suggests a different balance between these processes in the areas deforested during the final increment.

https://doi.org/10.5194/egusphere-2026-4899
Preprint. Discussion started: 11 September 2026

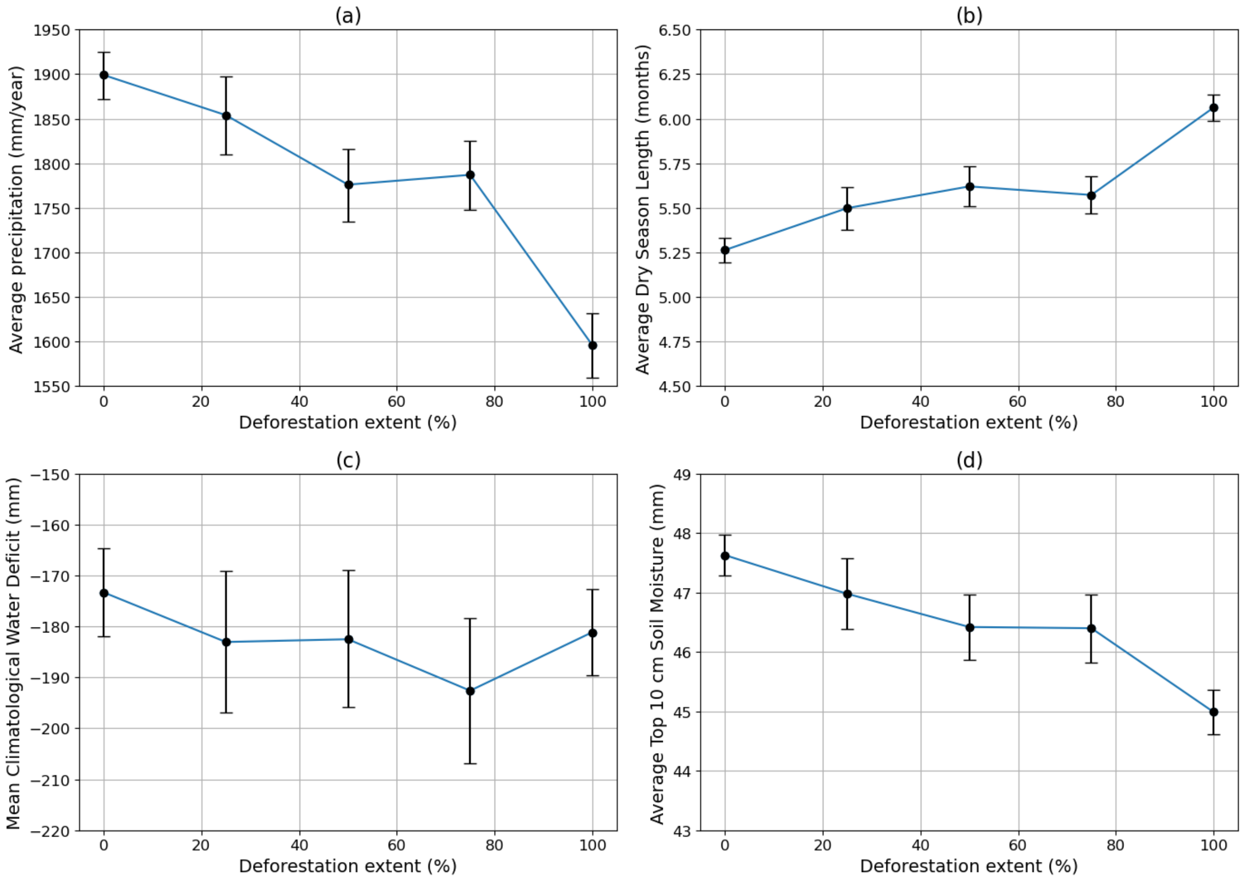

Figure 3 - Amazon average (a) Mean Annual Precipitation [MAP, in mm/year], (b) Dry Season Length [DSL, in months], (c) Mean Climatological Water Deficit [MCWD, in mm], and (d) Top 10 cm Soil Moisture [SM10, in mm] for all different deforestation scenarios under 2 degrees of global warming. Error bars indicate uncertainty of the mean calculation (here estimated as 2 * standard deviation of interannual variability).

Figure 4 shows that DSL presents the strongest regional responses to deforestation, with areas in central Amazon indicating severe and extreme changes (standardized anomaly > 2.0 and 2.5, respectively, as introduced in Sect. 2.1) as early as after 25% deforestation. Severe and extreme standardized anomalies spread all over the Amazon with increasing deforestation, as is the case for MAP and SM10. On the other hand, MCWD anomalies are mostly limited to moderate levels, even at high levels of deforestation.

https://doi.org/10.5194/egusphere-2026-4899
Preprint. Discussion started: 11 September 2026

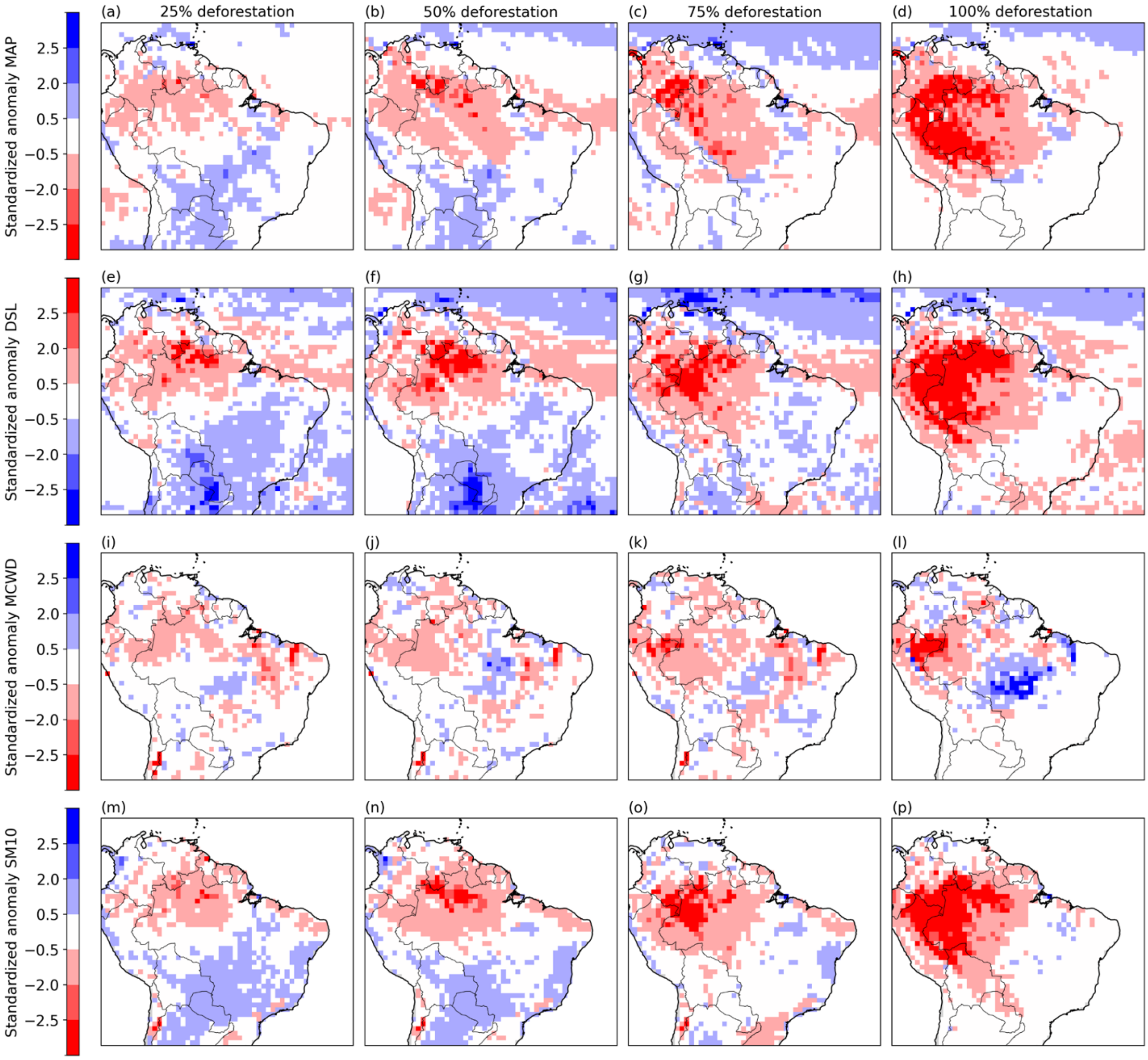

Figure 4 - Standardized anomalies (in units of standard deviation of the stableT_2K scenario, as described in the methods) of MAP (a-d), DSL (e-h), MCWD (i-l) and SM10 (m-p), under the 25% (first column), 50% (second column), 75% (third column) and 100% (fourth column) deforestation scenarios. This uses the stableT_2K scenario as a reference for anomalies, therefore considers deforestation-only effects.

Overall, DSL exhibited the largest response to deforestation relative to its standard deviation, followed by MAP and SM10. SM10 also showed a large response relative to its standard deviation, although it exhibited the smallest percentage change relative to its absolute value. For most indicators, the largest increases in hydroclimatic change occurred during the first 25% increment in deforestation, indicating a nonlinear response to forest loss. This pattern was particularly pronounced for DSL

https://doi.org/10.5194/egusphere-2026-4899
Preprint. Discussion started: 11 September 2026

and MAP, whose standardized changes were substantially larger during the initial stages of deforestation than during subsequent increments. This suggests that at deforestation levels approaching the approximately 18% accumulated deforestation reported in recent assessments of the Amazon (Hirota et al., 2021), both DSL and MAP already exhibited marked departures from their baseline variability.

3.2 Stress indicators in forested vs deforested areas

Figure 5 shows the average relative change in the four VHSI between consecutive deforestation levels for unchanged grid boxes (including intact forest and previously deforested areas) and newly deforested grid boxes. In newly deforested areas, precipitation decreases by more than 10% in every increment, whereas in unchanged areas it declines by less than 5% after the first 25% deforestation step and remains nearly stable thereafter. Given the model's horizontal resolution (~100 × 100 km), these results capture synoptic-scale rather than local-scale responses. A similar clear contrasting pattern consistent in every deforestation increment is not observed at the other indicators. SM10 also shows stronger reductions in changed gridboxes, but the percentual differences are much smaller. DSL increases more in unchanged forest in the first deforestation increment (with both categories increasing significantly), but this shifts to stronger deviations in changed areas in the further deforestation increments. MCWD also has both categories affected quite similarly in the first deforestation increment and different responses in the further deforestation increments. As deforestation progresses, MAP and SM10 reductions are strongest in newly deforested areas and nearby regions, while DSL, and MCWD exhibit substantial changes also in downwind areas. DSL is particularly noteworthy: beyond its significant increase, its anomalies spread extensively across the basin as deforestation advances. Unlike MAP and SM10, both DSL and MCWD are dry-season metrics, highly dependent on the rainy season onset. Therefore, the results suggest that deforestation exerts more far-reaching spatial impacts through dry-season intensification than through year-round changes such as those reflected in MAP.

https://doi.org/10.5194/egusphere-2026-4899
Preprint. Discussion started: 11 September 2026

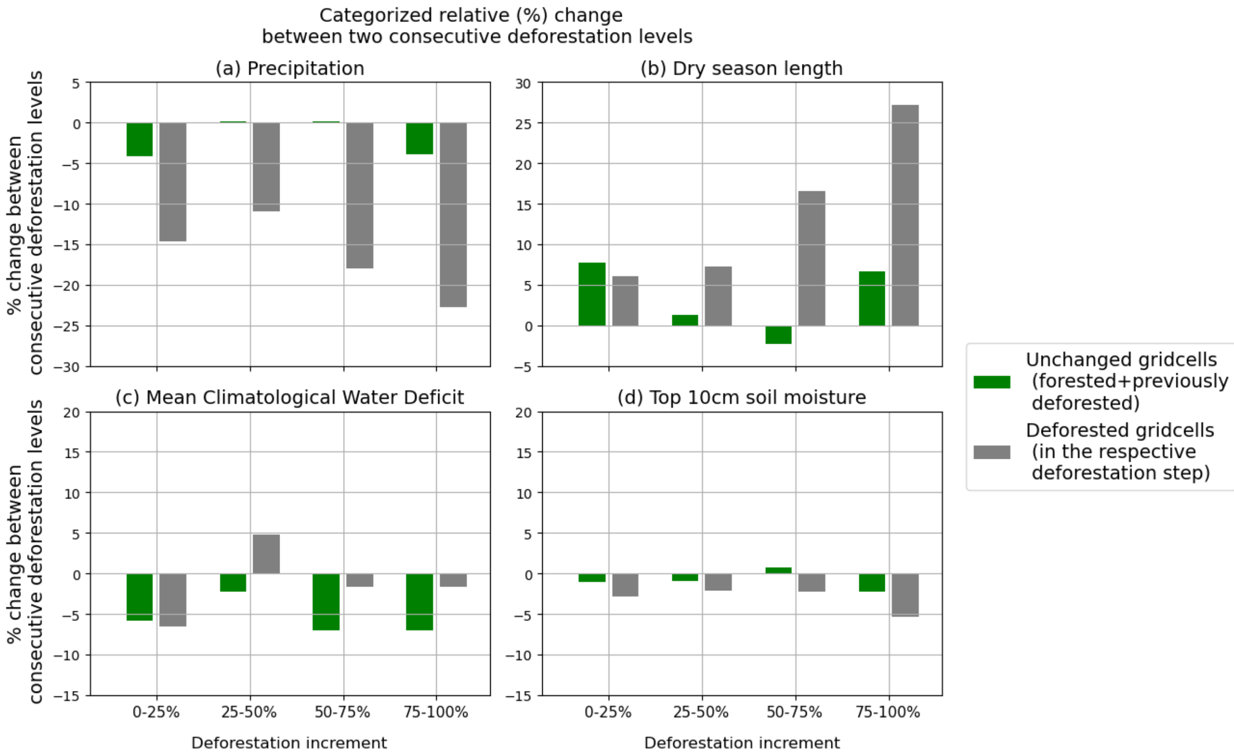

Figure 5 - Relative changes (in %) in MAP (a), DSL (b), MCWD (c) and SM10 (d) after each deforestation increment for the unchanged gridcells (where forest cover was not changed in the indicated deforestation increment) and the deforested gridcells (where forest has been removed in the indicated deforestation increment).

3.3 Effects of the changes in the vegetation hydroclimatic stress indicators on downstream forest stability

To assess how changes in VHSI may affect downstream areas, we quantified the fraction of remaining forest experiencing moderate, severe, and extreme stress under different deforestation scenarios. In this analysis, the reported percentages represent the affected forest area rather than the percentage reduction in the respective variable, as presented in previous sections. Figure 6 shows the fractions of deforested and significantly disturbed forest, in addition to the fraction of undisturbed forest, for the stableT_2K_ARF25 and stableT_2K_ARF50 scenarios using both stableT_2K and piControl as a reference for stability.

In the stableT_2K_ARF25 scenario (compared to stableT_2K), the deforestation-only effect has significantly disturbed 70% of the total forest. From this, 25% comes from deforestation and an additional 45% comes from hydroclimatic stress, meaning that only 30% of the forest is undisturbed, in this scenario. For the composite effect of the 2 degree warming effect and deforestation (stableT_2K_ARF25 compared to piControl), we find that 89% of the forest is significantly disturbed. Considering that 25% comes from forest removal, an additional 64% of the forest is under significant hydroclimatic stress, leaving only 11% of the forest as undisturbed. According to recent projections of deforestation and global warming (e.g.

https://doi.org/10.5194/egusphere-2026-4899
Preprint. Discussion started: 11 September 2026

Walker et al., 2019; Lee et al., 2021) there are high probabilities that values of 2 degree warming and 25% deforestation will be crossed before 2050, unless major measures of forest protection and mitigation are employed. In the stableT_2K_ARF50 scenario, we see that 82% of the forest is significantly disturbed in the deforestation-only comparison (50% deforested + 32% under hydroclimatic stress) and only 18% of the forest is undisturbed. This shows that the composite effect of 25% deforestation and 2 degree warming significantly affects a larger fraction of the forest than the deforestation-only effects of 50% deforestation. The composite effects of deforestation and warming under the stableT_2K_ARF50 scenario show that, in addition to the 50% of the forest removed, 40% of the forest is under significant hydroclimatic stress - a total of 90% of the forest significantly disturbed. The stableT_2K_ARF75 scenario (not shown) has more than 95% of the forest significantly disturbed for both deforestation-only and composite effects. Thus, all comparisons imply that a substantially larger fraction of the forest is significantly affected by hydroclimatic stress than is initially cleared, i.e. climatic effects of deforestation extend severely into other regions of the Amazon rainforest, putting them at risk of degradation. Combined with global warming of 2 degrees, only around one tenth of the forest remains undisturbed, even if only 25% or 50% had initially been cleared.

https://doi.org/10.5194/egusphere-2026-4899
Preprint. Discussion started: 11 September 2026

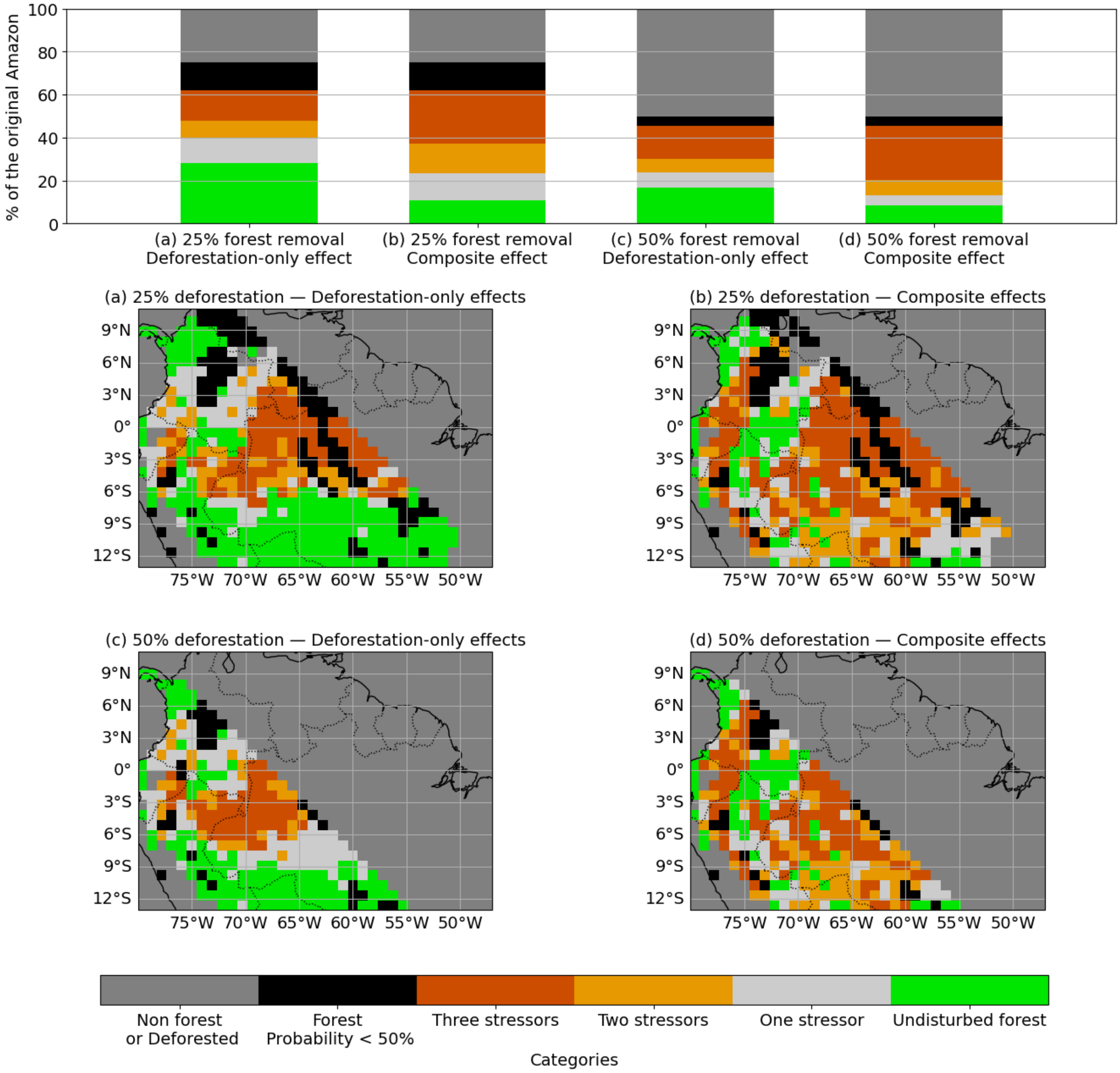

Figure 6 - Fraction of the Amazon rainforest that is significantly disturbed and that is undisturbed under 25% deforestation considering deforestation only (a) and the composite effect of deforestation and warming (b); same for 50% deforestation considering deforestation-only (c) and composite (d) effects. Each map and their associated column are two visualizations of the same data. Significant disturbance, as classified here, comes from deforestation (in gray), forest probability below 50% using the Mean Annual Precipitation (MAP) and the method by Hirota et a. (2011) (in black), or standardized anomalies > |0.5| for one, two or three of the other Vegetation Hydroclimatic Stress Indicators (DSL, MCWD and SM10) (in light gray, orange or red, respectively). Non forest refers to areas where forest cover was below 40% even in piControl.

https://doi.org/10.5194/egusphere-2026-4899
Preprint. Discussion started: 11 September 2026

Extreme standardized anomalies are found in smaller fractions of the forest, however, as they represent larger changes in the hydroclimatic indicators, they indicate areas exposed to an even stronger hydroclimatic risk. When considering only the areas with extreme standardized anomalies, the composite effects of stableT_2K_ARF25 leave 44% of the forest significantly disturbed (25% deforestation + 19% extreme hydroclimatic stress), while the deforestation-only scenario leaves 39% of the forest significantly disturbed (25% deforestation + 14% extreme hydroclimatic stress). For stableT_2K_ARF50, the composite effects leave 59% of the forest under significant disturbance (50% deforested + 9% extreme hydroclimatic stress), while under deforestation-only effects this represents 56% of the forest (50% deforested + 6% extreme hydroclimatic stress). For stableT_2K_ARF75 the values of disturbed forest are 80% and 79% for the composite and deforestation only effects, respectively. The maps show a notable feature that can be observed in the south of the Amazon in the stableT_2K_ARF25 scenario. The deforestation-only results show a large area in the south of the Amazon being undisturbed. However, when looking at the composite effects, this whole area is under significant stress. Also noticeable is the spread of areas with forest probability < 50% due to reduced MAP (according to Hirota et al., 2011), especially closer to the stripe where forest was removed. In the central Amazon region, the dark orange area indicates that SM10, DSL and MCWD show significant deviation from equilibrium in both deforestation-only and composite effects.

We also assessed the impacts of deforestation and warming by comparing the temporal mean of each VHSI variable at every Amazon grid box in each experiment (e.g. the grid-box mean in stableT_2K_ARF25) with the interannual distribution at the corresponding grid box in the respective reference simulation (piControl for the combined effects of warming and deforestation, and stableT_2K for deforestation-only effects). Specifically, we determined the percentile rank of the experiment's temporal mean within the reference simulation's interannual distribution at each grid box. This analysis quantifies how unusual the simulated (forced) mean state is relative to the range of natural (unforced) year-to-year variability expected at that location.

The same framework was applied to compare Amazon hydroclimatic conditions with those of the Cerrado, a tropical savanna south of the Amazon that represents a potential post-tipping analogue for the rainforest. The regional mean of each VHSI variable over the Cerrado (7°S–20°S, 60°W–45°W) was calculated from the piControl simulation and its percentile rank was determined relative to the interannual distribution at each Amazon grid box. Because two distinct regions were compared, the Cerrado regional mean was evaluated against the local temporal distribution of each Amazon grid box. This analysis assesses whether deforestation and warming shift Amazon hydroclimatic conditions toward—or beyond—those characteristic of the pre-industrial Cerrado, indicating increasing climatic similarity between the two regions - a potential indicator of a shift in the biome towards what is found in a tropical savanna.

Figure 7 summarizes this analysis for the four VHSI variables. The markers represent the Amazon-wide mean of the grid-box percentile ranks obtained using the procedure described above. Thus, a marker at the 60th percentile indicates that, on average across Amazon grid boxes, the scenario mean is higher than 60% of the corresponding reference interannual values.

https://doi.org/10.5194/egusphere-2026-4899
Preprint. Discussion started: 11 September 2026

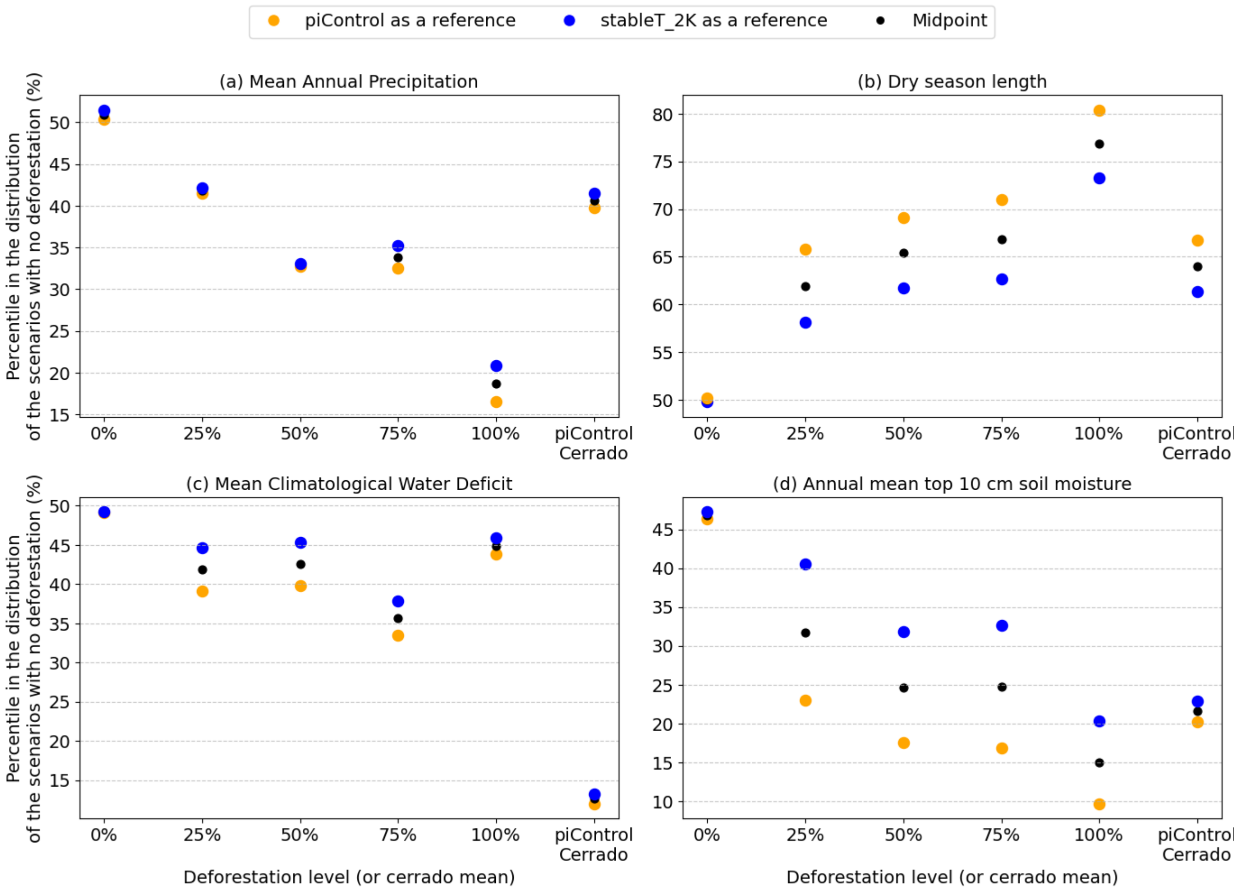

Figure 7 - Amazon-wide mean of the grid-box percentile ranks relative to the interannual distribution of the reference (no-deforestation) simulation (vertical axis). The horizontal axes show deforestation levels, with the final tick indicating the Cerrado mean under pre-industrial control. The blue marks represent the results with stableT_2K as a reference (deforestation-only effects for deforestation experiments) and the orange marks represent the results with piControl as a reference (composite effects for deforestation experiments) percentile bounds. The smaller black markers indicate the midpoint between the other two. Panels show: (a) Mean Annual Precipitation, (b) Dry Season Length, (c) Mean Climatological Water Deficit, and (d) Annual Mean top-10 cm Soil moisture.

At 25% deforestation, the mean DSL shifts to approximately the 60th percentile of its pre-deforestation distribution, representing a ~10% distributional shift. As the mean DSL distribution (like MAP) is approximately gaussian, we can use the shift to estimate how the distribution changes and with this estimate the changes in return times of certain DSL ranges. Using this approach we find that while this 10% shift in the distribution only slightly reduces the return period of average DSL conditions (from ~2.5 to ~2 years), a similar shift in the upper tail would substantially alter extremes; for example, a 10% shift around the 85th percentile could reduce return times from 20 to 6.7 years, effectively tripling the frequency of severe drought events. At 25% deforestation, the DSL percentile range already overlaps considerably with that of the pre-

https://doi.org/10.5194/egusphere-2026-4899
Preprint. Discussion started: 11 September 2026

industrial Cerrado, indicating that the Amazon may experience dry-season conditions comparable to those of the Cerrado prior to global warming. At 50% deforestation, Amazon DSL conditions can even exceed pre-industrial Cerrado levels. MAP exhibits a similar pattern.

MCWD also shows an approximately 10% mean deviation after 25% deforestation; however, because Cerrado MCWD deficits are substantially stronger than those in the Amazon, Amazon values do not reach pre-industrial Cerrado levels under any deforestation scenario. For SM10, overlap with Cerrado conditions emerges only after 50% deforestation. Larger separations between composite and deforestation-only markers indicate stronger additional warming effects, highlighting DSL and SM10 as the indicators most sensitive to the combined influence of deforestation and 2 °C warming.

4 Discussion

4.1 Implications of the experimental setup

This study performed idealized experiments of deforestation and warming. In the idealized deforestation setup, entire stripes of the forest in the northeastern Amazon were removed. According to the moisture recycling theory, it would be expected that deforestation reduces precipitation mostly downstream, resulting in a potential self-amplifying effect (e.g. Boers et al., 2017; Zemp et al., 2017). It should be noted that the model (like many Earth system models) shows a negative precipitation bias in the region of the Guianas. The simulated MAP reductions are hence likely also biased, that is, showing reductions significantly smaller than it would without the negative precipitation bias. This bias may also explain why precipitation, unlike the other three VHSI indicators, did not exhibit its strongest Amazon-wide decrease during the first 25% deforestation increment (2.3%) compared with the 25–50% increment (4.2%). As shown in Sect. 3.2 (Fig. 5), precipitation declines more strongly in newly deforested grid boxes than in unchanged ones. Because much of the deforestation during the first 25% increment overlaps the region with negative precipitation bias, the precipitation response during this stage is likely underestimated, and may in reality have exceeded that of the 25–50% increment.

In the real world, most of the deforestation occurs in the south-eastern parts of the Amazon (Berenguer et al., 2021). In our experiments, the MAP reduction was stronger in the areas where forest was removed, therefore, one can expect the stronger MAP reductions in the real world to occur in the south-eastern parts of the Amazon. Additionally, our results have shown that DSL, SM10 and MCWD affect larger areas than MAP, even in non-deforested regions - something that was already observed in the 2005, 2010 and 2015/16 droughts in the Amazon (Papastefanou, 2022) and tends to get worse, based on our results.

Regarding the model configuration, all experiments with intermediate deforestation (<100%) were conducted with dynamical vegetation enabled. Despite this, forest cover remained largely stable over the 60-year simulations, varying by less than 2% on the Amazon average (not shown). Locally, however, northern Amazon regions with a strong negative precipitation bias (MAP < 500 mm) exhibited forest cover increases of up to 10% (not shown). These areas had lost up to half of their forest cover during the spin-up phase (resulting in forest cover in the range of 45-65%), which was required to

https://doi.org/10.5194/egusphere-2026-4899
Preprint. Discussion started: 11 September 2026

equilibrate vegetation under the precipitation bias; the subsequent increase reflects partial recovery of this initial loss. Under such low MAP values, both forest persistence and recovery are highly unlikely. Empirical evidence from Hirota et al. (2011) shows that in more than 95% of global observations with MAP below 500 mm, forest cover is under 20% - way below the lowest values observed in our experiment with dynamical vegetation. The simulated forest distribution in specific MAP regimes is therefore unrealistic, which is consistent with previous claims that models tend to underrepresent abrupt vegetation shifts (Valdes, 2011; Liu et al., 2017).

4.2 Deforestation, warming and the hydroclimatic stress imposed on the Amazon rainforest

The following section focuses on three main aspects of the simulated hydroclimatic response to Amazon deforestation. First, we examine how deforestation induces hydroclimatic stress beyond the deforested areas, particularly when combined with global warming. Second, we discuss how changes in mean VHSIs imply an altered frequency and severity of hydroclimatic extremes across the Amazon. Finally, we discuss the extent of nonlinearity in the response of VHSI indicators to deforestation.

First, deforestation induces hydroclimatic stress well beyond the directly deforested regions. Although precipitation reductions in the model may be underestimated (following results from Sect. 2.3), it strongly affected deforested areas and their vicinity in comparison to non deforested areas, highlighting a contrast between local and non-local effects, also discussed in Sect. 3.2. Consequently, a large portion of the remaining forest under at least moderate hydroclimatic stress was affected primarily by changes in DSL, MCWD, or SM10, that is, by alterations in dry season length and intensity and their impacts on soil moisture. Our results are in line with previous deforestation studies in the Amazon (e.g. Sampaio et al., 2007; Nobre et al., 2009, Boysen et al., 2020), especially in terms of the dry season effects (e.g. Sampaio et al., 2007; Silveira et al., 2025). There is no clear consensus, however, on which areas would experience a larger precipitation decrease, as Boysen et al. (2020) has reported that some models have shown larger decreases in precipitation far from the deforested areas - supporting the hypothesis of the downwind effects of deforestation. In our study, these downwind effects are more pronounced in the intensity and length of the dry season, in comparison with MAP, which agrees with several studies that have already reported the increasing effects of longer and more intense dry periods in the Amazon rainforest associated with warming and deforestation in the last few decades (e.g. Fu et al., 2013; Marengo et al., 2021; Papastefanou et al., 2022; Silveira et al., 2025). In addition, recent strong droughts have already affected more than 50% of the Amazon basin (Papastefanou et al., 2022). In this context, another relevant result is the contrast between the deforestation-only and the composite effect. The composite effect of the stableT_2K_ARF25 scenario with warming affects a larger fraction of the forest than the deforestation-only effect of the stableT_2K_ARF50 scenario. This is in line with previous literature, which indicates that the composite effects of global warming and deforestation can increase the risk of stability loss by the rainforest (e.g. Lovejoy and Nobre, 2019; Flores et al., 2024; Wunderling et al., 2026). The direct comparison of the estimated effects puts in perspective the intensification of the composite effects (in comparison with the deforestation-only effects) and represents a novel contribution from the present study.

https://doi.org/10.5194/egusphere-2026-4899
Preprint. Discussion started: 11 September 2026

Second, changes in the VHSI reveal substantial shifts in mean values when compared to the undisturbed internal variability. This result implies a substantial change in the frequency of extreme conditions. Under 25% deforestation, DSL already shows similar values to what is observed in the Cerrado under pre-industrial conditions, with more extreme DSL values at higher deforestation levels. A similar result was found for MAP although MAP changes were more confined to the deforested areas, as discussed above. As an Amazon dieback has been speculated to result in a tropical savanna-like state (Nobre et al., 1991; Salati and Nobre, 1991; Lovejoy and Nobre, 2019, Flores et al., 2024), this climate analogy exercise lends some credibility to such a dieback scenario (assuming no alternative stable states that make tree cover depend on its history). It has to be pointed out however, that the Cerrado still shows much lower MCWD than the Amazon region for any deforestation level, and relatively low soil moisture; hence the analogy is by no means perfect. The shift in VHSI distributions also indicates a larger frequency of extreme events, which can cause significant hydroclimatic stress on the vegetation.

Finally, the response to deforestation is not perfectly linear, i.e. VHSI changes are not proportional with each additional 25% increment of forest area removal. Substantial changes in the four VHSI occurred already after the first 25% of deforestation, while they remain almost constant between 50% and 75% deforestation (or also 25% and 50% for the case of MCWD). This result shows that the location of deforestation matters; there could be areas in the Amazon where deforestation could have more severe impacts on the hydroclimate of the forest than others. This also relates with the discussion on the intensity of the effects downwind/upwind of deforestation, since according to moisture recycling theory deforestation can more significantly affect areas downwind than upwind.

These findings are highly relevant to forest stability and the potential for climate tipping transitions in the Amazon rainforest. In this context, evidence of increased greening during recent droughts in parts of the Amazon (Huete et al., 2006; Green et al., 2020) suggests that some regions have not yet experienced substantial hydroclimatic stress. However, Anderegg et al. (2019) show that vegetation in other areas is already exposed to climatic extremes beyond its adaptive capacity. The extent to which trees can adapt to intensifying hydroclimatic conditions remains uncertain. Nonetheless, our results of hydroclimatic changes, and the translation of MAP changes to forest probability, indicate that, in the absence of rapid adaptation, the combined effects of deforestation and global warming may cause substantial hydroclimatic stress, reducing tree cover in large areas of the forest - which could initiate a cascading dieback of the forest. The results show that this can occur at large scale already for forcings of 25% deforestation combined with 2 °C warming, levels that could be reached before 2050 (Walker et al., 2019; Lee et al., 2021), which could, depending on the adaptation from the vegetation, substantially undermine hydroclimatic conditionsand promote large-scale transitions towards a tropical savanna–like state across extensive areas of the Amazon. Notably, the Amazon has already reached approximately 17% deforestation by 2019 (Lovejoy and Nobre, 2019), although in a different region than assumed in our idealized study.

https://doi.org/10.5194/egusphere-2026-4899
Preprint. Discussion started: 11 September 2026

5 Conclusion

In this study we analyzed the response of four indicators that we defined as "Vegetation Hydroclimatic Stress Indicators" (VHSI), given their key role for forest stability: Mean Annual Precipitation (MAP), Dry Season Length (DSL), Mean Climatological Water Deficit (MCWD) and Top 10 cm Soil Moisture (SM10). Together, these indicators capture different dimensions of the hydroclimatic stress imposed on Amazon vegetation by deforestation and global warming.

Our results have shown significant effects of deforestation and global warming on the four VHSI analysed. We projected the fraction of Amazon forest exposed to significant hydroclimatic stress under increasing deforestation and warming scenarios. Forest areas were considered disturbed if they were deforested, exhibited MAP associated with less than 50% probability of tropical forest cover (Hirota et al., 2011), or showed at least moderate anomalies in the other VHSI indicators. We found that 25% deforestation alone could significantly disturb 70% of the forest, increasing to 89% when combined with 2 °C global warming. This exceeds the impacts of 50% deforestation alone (82%), highlighting the amplifying role of global warming on Amazon instability. Unless large mitigating efforts are made, the values of 25% deforestation and 2 degrees of global warming can be surpassed before the middle of the 21st century (Walker et al., 2019; Lee et al., 2021). Following the results from Papastefanou et al. (2022), that already have observed that the three most intense drought events in the first quarter of the 21st century have significantly affected more than 50% of the forest, we see that there is already an increasing trend in hydroclimatic stress on the Amazon rainforest, which can be dramatically intensified with the advancing deforestation and global warming. This has already created large areas in the southern and eastern Amazon that present MAP consistent with bimodal conditions between tropical forest and savanna (Flores et al., 2024). In this context, our results suggest that the composite effects of 25% deforestation and 2 degrees of global warming could greatly disturb the hydroclimatic conditionsof the Amazon rainforest. Without fast adaptation from the vegetation, this could have the potential to trigger cascading effects of forest dieback.

Our results have also shown that 25% of deforestation can shift the average DSL to values equivalent to approximately the 60th percentile. This shift plausibly suggests that extended drought events tend to increase in frequency under deforestation scenarios. If this results in a 10% shift in the whole gaussian distribution, as would be expected, this can represent an increase of 3 times or more in the frequency of DSL events longer than the 85th percentile in the equilibrium scenarios. This also implies that the DSL would reach values in the same range of those observed in the Cerrado, the tropical savanna biome south of the Amazon, under piControl. Moreover, precipitation reductions mostly occur in converted gridboxes (gridboxes where forest has been removed in the respective deforestation increment) and their vicinity, compared to untouched (downstream) or previously deforested (upstream) areas. To some extent, a similar behaviour occurs for SM10. In contrast, DSL and MCWD affect larger areas of the forest, without a clear distinction between forested and deforested areas. As a result, reduction in precipitation can pose a large threat to the areas in the Amazon where deforestation is higher, while DSL and MCWD affect larger areas of the forest.

These results contribute to the understanding of the potential hydroclimatic stress that the Amazon rainforest could be exposed to under future deforestation and global warming scenarios. With the still advancing deforestation and global warming, future research should continue to address all open questions regarding the stability of the Amazon rainforest and the potential climatic, economical, biological, social and cultural impacts of critical transitions. We believe that the reproduction of the same experiments by several ESMs and convection permitting models could greatly contribute to the robustness of the estimates presented for the scenarios considered in this study and other potential future scenarios. We also believe that further studies on the adaptability of the trees in the Amazon rainforest would be of major importance to increase the confidence in the existence and in the critical thresholds in deforestation and global warming levels.

Code and data availability

Data from the simulations without any deforestation and with complete deforestation are available at doi.org/10.5281/zenodo.16784935. Data from the intermediate deforestation scenarios (25%, 50% and 75% deforestation) are available in the ClimTip project storage in the Deutsches Klimarechenzentrum (DKRZ; project bm1404), and can be provided via the DKRZ system Levante or externally under request. The precipitation data from GPCC was downloaded from doi.org/10.5676/DWD_GPCC/MONTHLY_V2025_050. The CMIP6 data was acquired via the DKRZ archive, assessed directly via the DKRZ High Performance Computing system Levante.

Author Contributions

LFC, SB and JP designed the experiments and LFC performed the simulations. LFC organized the manuscript methods with contributions from all co-authors. All authors contributed to the analysis. LFC prepared the manuscript with contributions from all co-authors.

Competing interests

The authors declare that they have no conflict of interest.

Acknowledgements

This is ClimTip contribution #172; the ClimTip project has received funding from the European Union's Horizon Europe research and innovation programme under grant agreement No. 101137601: Funded by the European Union. Views and opinions expressed are however those of the authors only and do not necessarily reflect those of the European Union or the European Climate, Infrastructure and Environment Executive Agency (CINEA). Neither the European Union nor the granting authority can be held responsible for them. This work used resources of the Deutsches Klimarechenzentrum (DKRZ) granted by its Scientific Steering Committee (WLA) under project ID bm1404.

Financial Support

The ClimTip project has received funding from the European Union's Horizon Europe research and innovation programme under grant agreement No. 101137601: Funded by the European Union.

References

Aleixo, I., Norris, D., Hemerik, L., Barbosa, A., Prata, E., Costa, F., and Poorter, L.: Amazonian rainforest tree mortality driven by climate and functional traits, *Nature Climate Change*, 9(5), 384–388, https://doi.org/10.1038/s41558-019-0458-0, 2019.

Allen, C. D., Macalady, A. K., Chenchouni, H., Bachelet, D., McDowell, N., Vennetier, M., Kitzberger, T., Rigling, A., Breshears, D. D., Hogg, E. H. (Ted), Gonzalez, P., Fensham, R., Zhang, Z., Castro, J., Demidova, N., Lim, J.-H., Allard, G., Running, S. W., Semerci, A., and Cobb, N.: A global overview of drought and heat-induced tree mortality reveals emerging climate change risks for forests, *Forest Ecology and Management*, 259(4), 660–684, https://doi.org/10.1016/j.foreco.2009.09.001, 2010.

Anderegg, W. R. L., Anderegg, L. D. L., Kerr, K. L., and Trugman, A. T.: Widespread drought-induced tree mortality at dry range edges indicates that climate stress exceeds species' compensating mechanisms, *Global Change Biology*, 25(11), 3793–3802, https://doi.org/10.1111/gcb.14771, 2019.

Aragão, L. E. O. C., Malhi, Y., Roman-Cuesta, R. M., Saatchi, S., Anderson, L. O., and Shimabukuro, Y. E.: Spatial patterns and fire response of recent Amazonian droughts, *Geophysical Research Letters*, 34(7), 2006GL028946, https://doi.org/10.1029/2006GL028946, 2007.

Berenguer, E., Armenteras, D., Lees, A. C., Smith, C. C., Fearnside, P., Nascimento, N., Alencar, A., Almeida, C., Aragão, L. E. O., Barlow, J., Bilbao, B., Brando, P. M., Bynoe, P., Finer, M., Flores, B. M., Jenkins, C. N., Silva Junior, C. H. L., Souza, C., and García-Villacorta, R.: Chapter 19: Drivers and ecological impacts of deforestation and forest degradation, in: Science Panel for the Amazon, *Amazon Assessment Report 2021*, 1st ed., UN Sustainable Development Solutions Network (SDSN), https://doi.org/10.55161/AIZJ1133, 2021.

Boers, N., Marwan, N., Barbosa, H. M. J., and Kurths, J.: A deforestation-induced tipping point for the South American monsoon system, *Scientific Reports*, 7(1), 41489, https://doi.org/10.1038/srep41489, 2017.

Boysen, L. R., Brovkin, V., Pongratz, J., Lawrence, D. M., Lawrence, P., Vuichard, N., Peylin, P., Liddicoat, S., Hajima, T., Zhang, Y., Rocher, M., Delire, C., Séférian, R., Arora, V. K., Nieradzik, L., Anthoni, P., Thiery, W., Laguë, M. M., Lawrence, D., and Lo, M.-H.: Global climate response to idealized deforestation in CMIP6 models, *Biogeosciences*, 17(22), 5615–5638, https://doi.org/10.5194/bg-17-5615-2020, 2020.

Bultan, S., Moustakis, Y., Bathiany, S., Boers, N., Ganzenmüller, R., Gyuleva, G., and Pongratz, J.: Amazon forest faces severe decline under the dual pressures of anthropogenic climate change and land-use change, *Proceedings of the National Academy of Sciences*, 122(50), e2418813122, https://doi.org/10.1073/pnas.2418813122, 2025.

Cattelan, L. G., Mattos, C. R. C., and Hirota, M.: Unraveling divergences: Disagreement between precipitation datasets and stations in tropical South America, *Environmental Research Letters*, 20(10), 104043, https://doi.org/10.1088/1748-9326/ae02aa, 2025.

Chagnon, F. J. F. and Bras, R. L.: Contemporary climate change in the Amazon, *Geophysical Research Letters*, 32(13), 2005GL022722, https://doi.org/10.1029/2005GL022722, 2005.

https://doi.org/10.5194/egusphere-2026-4899
Preprint. Discussion started: 11 September 2026

Chambers, J. Q., Nogueira Lima, A. J., Pastorello, G., Gimenez, B. O., Meng, L., Dyer, L. A., Feng, Y., Santos Da Silva, C., Costa De Oliveira, R., Weber, A., Koven, C., Negrón-Juárez, R., Spanner, G. C., Gaui, T. D., Fontes, C. G., De Araújo, A. C., McDowell, N., Leung, R., Marra, D. M., … Higuchi, N.: Hot droughts in the Amazon provide a window to a future hypertropical climate, *Nature*, 649(8099), 1190–1196, https://doi.org/10.1038/s41586-025-09728-y, 2026.

Collow, A. B. M., Miller, M. A., and Trabachino, L. C.: Cloudiness over the Amazon rainforest: Meteorology and thermodynamics, *Journal of Geophysical Research: Atmospheres*, 121(13), 7990–8005, https://doi.org/10.1002/2016JD024848, 2016.

Cox, P. M., Betts, R. A., Collins, M., Harris, P. P., Huntingford, C., and Jones, C. D.: Amazonian forest dieback under climate-carbon cycle projections for the 21st century, *Theoretical and Applied Climatology*, 78(1–3), https://doi.org/10.1007/s00704-004-0049-4, 2004.

Cui, J., Piao, S., Huntingford, C., Wang, T., and Spracklen, D. V.: Historical deforestation drives strong rainfall decline across the southern Amazon basin, *Nature Communications*, 17(1), 1642, https://doi.org/10.1038/s41467-026-68361-z, 2026.

da Mota, M. A. S. and Nobre, C.: *Relação da variabilidade da Energia Potencial Convectiva Disponível (CAPE) com a Precipitação e a Alta da Bolívia durante a campanha "Wet-AMC/LBA"*, 2006.

Eltahir, E. A. B.: Role of vegetation in sustaining large-scale atmospheric circulations in the tropics, *Journal of Geophysical Research: Atmospheres*, 101(D2), 4255–4268, https://doi.org/10.1029/95JD03632, 1996.

Eltahir, E. A. B. and Bras, R. L.: Precipitation recycling in the Amazon basin, *Quarterly Journal of the Royal Meteorological Society*, 120(518), 861–880, https://doi.org/10.1002/qj.49712051806, 1994.

Esquivel-Muelbert, A., Phillips, O. L., Brienen, R. J. W., Fauset, S., Sullivan, M. J. P., Baker, T. R., Chao, K.-J., Feldpausch, T. R., Gloor, E., Higuchi, N., Houwing-Duistermaat, J., Lloyd, J., Liu, H., Malhi, Y., Marimon, B., Marimon Junior, B. H., Monteagudo-Mendoza, A., Poorter, L., Silveira, M., … Galbraith, D.: Tree mode of death and mortality risk factors across Amazon forests, *Nature Communications*, 11(1), 5515, https://doi.org/10.1038/s41467-020-18996-3, 2020.

Ferreira, G. W. S. and Reboita, M. S.: A New Look into the South America Precipitation Regimes: Observation and Forecast, *Atmosphere*, 13(6), 873, https://doi.org/10.3390/atmos13060873, 2022.

Fisch, G., Marengo, J. A., and Nobre, C. A.: Uma revisão geral sobre o clima da Amazônia, *Acta Amazonica*, 28(2), 101–101, https://doi.org/10.1590/1809-43921998282126, 1998.

Flores, B. M., Montoya, E., Sakschewski, B., Nascimento, N., Staal, A., Betts, R. A., Levis, C., Lapola, D. M., Esquível-Muelbert, A., Jakovac, C., Nobre, C. A., Oliveira, R. S., Borma, L. S., Nian, D., Boers, N., Hecht, S. B., Ter Steege, H., Arieira, J., Lucas, I. L., … Hirota, M.: Critical transitions in the Amazon forest system, *Nature*, 626(7999), 555–564, https://doi.org/10.1038/s41586-023-06970-0, 2024.

Fu, R., Yin, L., Li, W., Arias, P. A., Dickinson, R. E., Huang, L., Chakraborty, S., Fernandes, K., Liebmann, B., Fisher, R., and Myneni, R. B.: Increased dry-season length over southern Amazonia in recent decades and its implication for future climate projection, *Proceedings of the National Academy of Sciences*, 110(45), 18110–18115, https://doi.org/10.1073/pnas.1302584110, 2013.

Geoffroy, O., Saint-Martin, D., Olivié, D. J. L., Voldoire, A., Bellon, G., and Tytéca, S.: Transient Climate Response in a Two-Layer Energy-Balance Model. Part I: Analytical Solution and Parameter Calibration Using CMIP5 AOGCM Experiments, *Journal of Climate*, 26(6), 1841–1857, https://doi.org/10.1175/JCLI-D-12-00195.1, 2013.

https://doi.org/10.5194/egusphere-2026-4899
Preprint. Discussion started: 11 September 2026

Good, S. P., Noone, D., and Bowen, G.: Hydrologic connectivity constrains partitioning of global terrestrial water fluxes, *Science*, 349(6244), 175–177, https://doi.org/10.1126/science.aaa5931, 2015.

Green, J. K., Berry, J., Ciais, P., Zhang, Y., and Gentine, P.: Amazon rainforest photosynthesis increases in response to atmospheric dryness, *Science Advances*, 6(47), eabb7232, https://doi.org/10.1126/sciadv.abb7232, 2020.

Grossiord, C., Buckley, T. N., Cernusak, L. A., Novick, K. A., Poulter, B., Siegwolf, R. T. W., Sperry, J. S., and McDowell, N. G.: Plant responses to rising vapor pressure deficit, *New Phytologist*, 226(6), 1550–1566, https://doi.org/10.1111/nph.16485, 2020.

Guan, K., Pan, M., Li, H., Wolf, A., Wu, J., Medvigy, D., Caylor, K. K., Sheffield, J., Wood, E. F., Malhi, Y., Liang, M., Kimball, J. S., Saleska, S. R., Berry, J., Joiner, J., and Lyapustin, A. I.: Photosynthetic seasonality of global tropical forests constrained by hydroclimate, *Nature Geoscience*, 8(4), 284–289, https://doi.org/10.1038/ngeo2382, 2015.

Gutjahr, O., Putrasahan, D., Lohmann, K., Jungclaus, J. H., Von Storch, J.-S., Brüggemann, N., Haak, H., and Stössel, A.: Max Planck Institute Earth System Model (MPI-ESM1.2) for the High-Resolution Model Intercomparison Project (HighResMIP), *Geoscientific Model Development*, 12(7), 3241–3281, https://doi.org/10.5194/gmd-12-3241-2019, 2019.

Henderson-Sellers, A. and Gornitz, V.: Possible climatic impacts of land cover transformations, with particular emphasis on tropical deforestation, *Climatic Change*, 6(3), 231–257, https://doi.org/10.1007/BF00142475, 1984.

Hirota, M., Flores, B. M., Betts, R., Borma, L. S., Esquivel-Muelbert, A., Jakovac, C., Lapola, D. M., Montoya, E., Oliveira, R. S., and Sakschewski, B.: Chapter 24: Resilience of the Amazon forest to global changes: Assessing the risk of tipping points, in: Science Panel for the Amazon, *Amazon Assessment Report 2021*, 1st ed., UN Sustainable Development Solutions Network (SDSN), https://doi.org/10.55161/QPYS9758, 2021.

Hirota, M., Holmgren, M., Van Nes, E. H., and Scheffer, M.: Global Resilience of Tropical Forest and Savanna to Critical Transitions, *Science*, 334(6053), 232–235, https://doi.org/10.1126/science.1210657, 2011.

Hu, Q., Li, T., Deng, X., Wu, T., Zhai, P., Huang, D., Fan, X., Zhu, Y., Lin, Y., Xiao, X., Chen, X., Zhao, X., Wang, L., and Qin, Z.: Intercomparison of global terrestrial carbon fluxes estimated by MODIS and Earth system models, *Science of The Total Environment*, 810, 152231, https://doi.org/10.1016/j.scitotenv.2021.152231, 2022.

Huete, A. R., Didan, K., Shimabukuro, Y. E., Ratana, P., Saleska, S. R., Hutyra, L. R., Yang, W., Nemani, R. R., and Myneni, R.: Amazon rainforests green-up with sunlight in dry season, *Geophysical Research Letters*, 33(6), 2005GL025583, https://doi.org/10.1029/2005GL025583, 2006.

Jones, C., Lowe, J., Liddicoat, S., and Betts, R.: Committed terrestrial ecosystem changes due to climate change, *Nature Geoscience*, 2(7), 484–487, https://doi.org/10.1038/ngeo555, 2009.

Lean, J. and Rowntree, P. R.: A GCM simulation of the impact of Amazonian deforestation on climate using an improved canopy representation, *Quarterly Journal of the Royal Meteorological Society*, 119(511), 509–530, https://doi.org/10.1002/qj.49711951109, 1993.

Lean, J. and Warrilow, D. A.: Simulation of the regional climatic impact of Amazon deforestation, *Nature*, 342(6248), 411–413, https://doi.org/10.1038/342411a0, 1989.

Lee, J.-Y., Marotzke, J., Bala, G., Cao, L., Susanna, C., and Dunne, J.: *Climate Change 2021 – The Physical Science Basis: Working Group I Contribution to the Sixth Assessment Report of the Intergovernmental Panel on Climate Change*, 1st ed., Cambridge University Press, https://doi.org/10.1017/9781009157896, 2023.

https://doi.org/10.5194/egusphere-2026-4899
Preprint. Discussion started: 11 September 2026

Lewis, S. L., Brando, P. M., Phillips, O. L., Van Der Heijden, G. M. F., and Nepstad, D.: The 2010 Amazon Drought, *Science*, 331(6017), 554–554, https://doi.org/10.1126/science.1200807, 2011.

Liu, W., Xie, S.-P., Liu, Z., and Zhu, J.: Overlooked possibility of a collapsed Atlantic Meridional Overturning Circulation in warming climate, *Science Advances*, 3(1), e1601666, https://doi.org/10.1126/sciadv.1601666, 2017.

Lovejoy, T. E. and Nobre, C.: Amazon tipping point: Last chance for action, *Science Advances*, 5(12), eaba2949, https://doi.org/10.1126/sciadv.aba2949, 2019.

Mantova, M., Herbette, S., Cochard, H., and Torres-Ruiz, J. M.: Hydraulic failure and tree mortality: From correlation to causation, *Trends in Plant Science*, 27(4), 335–345, https://doi.org/10.1016/j.tplants.2021.10.003, 2022.

Marengo, J. A., Espinoza, J.-C., Esquivel-Muelbert, Lapola, D. M., Anderson, E., Armenteras, D., Bilbao, B., Fleischmann, Guayasamin, J. M., and Libonati: *CHAPTER 1 Amazon Connections from Regional to Global Impacts and Vulnerabilities*, 2025.

Marengo, J. A., Espinoza, J.-C., Fu, R., Jimenez Muñoz, J. C., Muniz Alves, L., Ribeiro Da Rocha, H., and Schongart, J.: Chapter 22: Long-term variability, extremes, and changes in temperature and hydro meteorology, in: Science Panel for the Amazon, *Amazon Assessment Report 2021*, 1st ed., UN Sustainable Development Solutions Network (SDSN), https://doi.org/10.55161/ZGJG8060, 2021.

Mauritsen, T., Bader, J., Becker, T., Behrens, J., Bittner, M., Brokopf, R., Brovkin, V., Claussen, M., Crueger, T., Esch, M., Fast, I., Fiedler, S., Fläschner, D., Gayler, V., Giorgetta, M., Goll, D. S., Haak, H., Hagemann, S., Hedemann, C., … Roeckner, E.: Developments in the MPI-M Earth System Model version 1.2 (MPI-ESM1.2) and Its Response to Increasing CO2, *Journal of Advances in Modeling Earth Systems*, 11(4), 998–1038, https://doi.org/10.1029/2018MS001400, 2019.

McDowell, N., Allen, C. D., Anderson-Teixeira, K., Brando, P., Brienen, R., Chambers, J., Christoffersen, B., Davies, S., Doughty, C., Duque, A., Espirito-Santo, F., Fisher, R., Fontes, C. G., Galbraith, D., Goodsman, D., Grossiord, C., Hartmann, H., Holm, J., Johnson, D. J., … Xu, X.: Drivers and mechanisms of tree mortality in moist tropical forests, *New Phytologist*, 219(3), 851–869, https://doi.org/10.1111/nph.15027, 2018.

Müller, W. A., Jungclaus, J. H., Mauritsen, T., Baehr, J., Bittner, M., Budich, R., Bunzel, F., Esch, M., Ghosh, R., Haak, H., Ilyina, T., Kleine, T., Kornblueh, L., Li, H., Modali, K., Notz, D., Pohlmann, H., Roeckner, E., Stemmler, I., … Marotzke, J.: A Higher-resolution Version of the Max Planck Institute Earth System Model (MPI-ESM1.2-HR), *Journal of Advances in Modeling Earth Systems*, 10(7), 1383–1413, https://doi.org/10.1029/2017MS001217, 2018.

Muller-Landau, H. C., Cushman, K. C., Arroyo, E. E., Martinez Cano, I., Anderson-Teixeira, K. J., and Backiel, B.: Patterns and mechanisms of spatial variation in tropical forest productivity, woody residence time, and biomass, *New Phytologist*, 229(6), 3065–3087, https://doi.org/10.1111/nph.17084, 2021.

Negri, A. J., Adler, R. F., Xu, L., and Surratt, J.: The Impact of Amazonian Deforestation on Dry Season Rainfall, *Journal of Climate*, 17(6), 1306–1319, https://doi.org/10.1175/1520-0442(2004)017%3C1306:TIOADO%3E2.0.CO;2, 2004.

Nepstad, D. C., De Carvalho, C. R., Davidson, E. A., Jipp, P. H., Lefebvre, P. A., Negreiros, G. H., Da Silva, E. D., Stone, T. A., Trumbore, S. E., and Vieira, S.: The role of deep roots in the hydrological and carbon cycles of Amazonian forests and pastures, *Nature*, 372(6507), 666–669, https://doi.org/10.1038/372666a0, 1994.

Nepstad, D. C., Tohver, I. M., Ray, D., Moutinho, P., and Cardinot, G.: MORTALITY OF LARGE TREES AND LIANAS FOLLOWING EXPERIMENTAL DROUGHT IN AN AMAZON FOREST, *Ecology*, 88(9), 2259–2269, https://doi.org/10.1890/06-1046.1, 2007.

https://doi.org/10.5194/egusphere-2026-4899
Preprint. Discussion started: 11 September 2026

Nian, D., Bathiany, S., Sakschewski, B., Drüke, M., Blaschke, L., Ben-Yami, M., Von Bloh, W., and Boers, N.: Rainfall seasonality dominates critical precipitation threshold for the Amazon forest in the LPJmL vegetation model, *Science of The Total Environment*, 947, 174378, https://doi.org/10.1016/j.scitotenv.2024.174378, 2024.

Nobre, C. A., Sampaio, G., Borma, L. S., Castilla-Rubio, J. C., Silva, J. S., and Cardoso, M.: Land-use and climate change risks in the Amazon and the need of a novel sustainable development paradigm, *Proceedings of the National Academy of Sciences*, 113(39), 10759–10768, https://doi.org/10.1073/pnas.1605516113, 2016.

Nobre, C. A., Sellers, P. J., and Shukla, J.: Amazonian Deforestation and Regional Climate Change, *Journal of Climate*, 4(10), 957–988, https://doi.org/10.1175/1520-0442(1991)004%3C0957:ADARCC%3E2.0.CO;2, 1991.

Nobre, P., Malagutti, M., Urbano, D. F., De Almeida, R. A. F., and Giarolla, E.: Amazon Deforestation and Climate Change in a Coupled Model Simulation, *Journal of Climate*, 22(21), 5686–5697, https://doi.org/10.1175/2009JCLI2757.1, 2009.

Papastefanou, P., Zang, C. S., Angelov, Z., De Castro, A. A., Jimenez, J. C., De Rezende, L. F. C., Ruscica, R. C., Sakschewski, B., Sörensson, A. A., Thonicke, K., Vera, C., Viovy, N., Von Randow, C., and Rammig, A.: Recent extreme drought events in the Amazon rainforest: Assessment of different precipitation and evapotranspiration datasets and drought indicators, *Biogeosciences*, 19(16), 3843–3861, https://doi.org/10.5194/bg-19-3843-2022, 2022.

Parry, I., Ritchie, P., and Cox, P.: *Evidence of Amazon rainforest dieback in CMIP6 models*, https://doi.org/10.48550/ARXIV.2203.11744, 2022.

Reick, C. H., Gayler, V., Goll, D., Hagemann, S., Heidkamp, M., Nabel, J. E. M. S., Raddatz, T., Roeckner, E., Schnur, R., and Wilkenskjeld, S.: *JSBACH 3 - The land component of the MPI Earth System Model: Documentation of version 3.2*, 4990986, https://doi.org/10.17617/2.3279802, 2021.

Salati, E. and Nobre, C. A.: Possible climatic impacts of tropical deforestation, *Climatic Change*, 19(1–2), 177–196, https://doi.org/10.1007/BF00142225, 1991.

Sampaio, G., Nobre, C., Costa, M. H., Satyamurty, P., Soares-Filho, B. S., and Cardoso, M.: Regional climate change over eastern Amazonia caused by pasture and soybean cropland expansion, *Geophysical Research Letters*, 34(17), 2007GL030612, https://doi.org/10.1029/2007GL030612, 2007.

Schneider, U., Hänsel, S., Finger, P., Rustemeier, E., and Ziese, M.: *GPCC Full Data Monthly Version 2022 at 0.5°: Monthly Land-Surface Precipitation from Rain-Gauges built on GTS-based and Historic Data: Globally Gridded Monthly Totals*, Version 2022, Global Precipitation Climatology Centre (GPCC) at Deutscher Wetterdienst, https://doi.org/10.5676/DWD_GPCC/FD_M_V2022_050, 2022.

Shukla, J., Nobre, C., and Sellers, P.: Amazon Deforestation and Climate Change, *Science*, 247(4948), 1322–1325, https://doi.org/10.1126/science.247.4948.1322, 1990.

Silveira, M. V. F., Keys, P. W., Ruhoff, A., Artaxo, P., Costa, M. H., Anderson, L. O., Adami, M., Von Randow, C., and Aragão, L. E. O. C.: Observed shifts in regional climate linked to Amazon deforestation, *Communications Earth & Environment*, 6(1), 948, https://doi.org/10.1038/s43247-025-02900-2, 2025.

Staal, A., Tuinenburg, O. A., Bosmans, J. H. C., Holmgren, M., Van Nes, E. H., Scheffer, M., Zemp, D. C., and Dekker, S. C.: Forest-rainfall cascades buffer against drought across the Amazon, *Nature Climate Change*, 8(6), 539–543, https://doi.org/10.1038/s41558-018-0177-y, 2018.

https://doi.org/10.5194/egusphere-2026-4899
Preprint. Discussion started: 11 September 2026

Stevens, B., Giorgetta, M., Esch, M., Mauritsen, T., Crueger, T., Rast, S., Salzmann, M., Schmidt, H., Bader, J., Block, K., Brokopf, R., Fast, I., Kinne, S., Kornblueh, L., Lohmann, U., Pincus, R., Reichler, T., and Roeckner, E.: Atmospheric component of the MPI-M Earth System Model: ECHAM6, *Journal of Advances in Modeling Earth Systems*, 5(2), 146–172, https://doi.org/10.1002/jame.20015, 2013.

Valdes, P.: Built for stability, *Nature Geoscience*, 4(7), 414–416, https://doi.org/10.1038/ngeo1200, 2011.

Walker, R. T., Simmons, C., Arima, E., Galvan-Miyoshi, Y., Antunes, A., Waylen, M., and Irigaray, M.: Avoiding Amazonian Catastrophes: Prospects for Conservation in the 21st Century, *One Earth*, 1(2), 202–215, https://doi.org/10.1016/j.oneear.2019.09.009, 2019.

Williams, M., Milodowski, D. T., Smallman, T. L., Dexter, K. G., Hegerl, G. C., McNicol, I. M., O'Sullivan, M., Roesch, C. M., Ryan, C. M., Sitch, S., and Valade, A.: Precipitation–fire functional interactions control biomass stocks and carbon exchanges across the world's largest savanna, *Biogeosciences*, 22(6), 1597–1614, https://doi.org/10.5194/bg-22-1597-2025, 2025.

Winckler, J., Reick, C. H., and Pongratz, J.: Robust Identification of Local Biogeophysical Effects of Land-Cover Change in a Global Climate Model, *Journal of Climate*, 30(3), 1159–1176, https://doi.org/10.1175/JCLI-D-16-0067.1, 2017.

Wood, R. A., Batthiany, S., Boers, N., Brovkin, V., Ferreira Correa, L., Georgievski, G., Jackson, L. C., Jones, C., Liddicoat, S., Loriani, S., Patrizio, C. R., Pongratz, J., Ringer, M. A., and von der Heydt, A. S.: *Control of global temperature in concentration-driven climate models (June 2026)*, https://doi.org/10.5281/ZENODO.20560920, 2026.

Wunderling, N., Sakschewski, B., Rockström, J., Flores, B. M., Hirota, M., and Staal, A.: Deforestation-induced drying lowers Amazon climate threshold, *Nature*, https://doi.org/10.1038/s41586-026-10456-0, 2026.

Xu, H., Lian, X., Slette, I. J., Yang, H., Zhang, Y., Chen, A., and Piao, S.: Rising ecosystem water demand exacerbates the lengthening of tropical dry seasons, *Nature Communications*, 13(1), 4093, https://doi.org/10.1038/s41467-022-31826-y, 2022.

Zemp, D. C., Schleussner, C.-F., Barbosa, H. M. J., Hirota, M., Montade, V., Sampaio, G., Staal, A., Wang-Erlandsson, L., and Rammig, A.: Self-amplified Amazon forest loss due to vegetation-atmosphere feedbacks, *Nature Communications*, 8(1), 14681, https://doi.org/10.1038/ncomms14681, 2017.